The Abdus Salam International Centre for Theoretical Physics

2454-9

Joint ICTP-IAEA Workshop on Advanced Synchrotron Radiation Based X-ray Spectrometry Techniques

22 - 26 April 2013

Confocal Microscopy for 3D elemental imaging and Analysis

A. Karydas

IAEA Laboratories, Seibersdorf
Austria

Confocal Microscopy for 3D elemental imaging and Analysis

Andreas Karydas,
Nuclear Spectrometry and Applications Laboratory
IAEA Laboratories, Seibersdorf
A.Karydas@iaea.org

X-rays Optics

Refractive index $\Rightarrow \quad n = \dfrac{c}{u_p}$

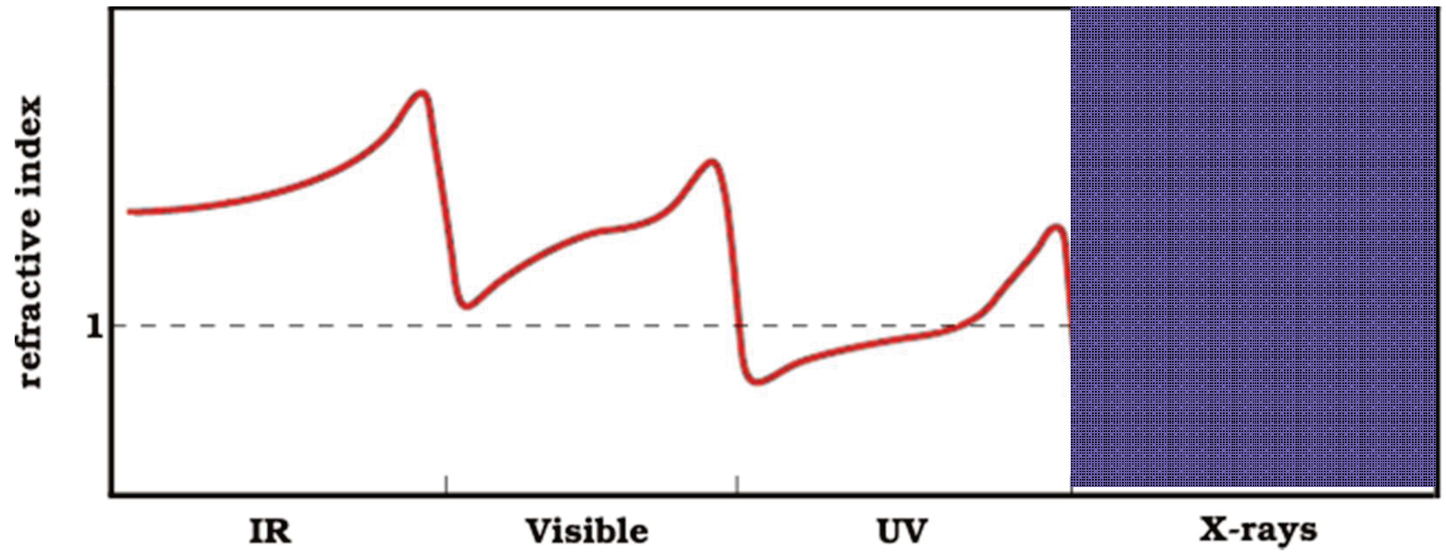

$$n = 1 - \delta - i\beta$$

$$\delta = \frac{414.7}{E^2} \cdot \frac{Z_\rho \cdot \rho}{A}$$

phase term

$$\beta = \frac{\lambda}{4\pi}\tau$$

attenuation term

X-Ray optics: External total reflection

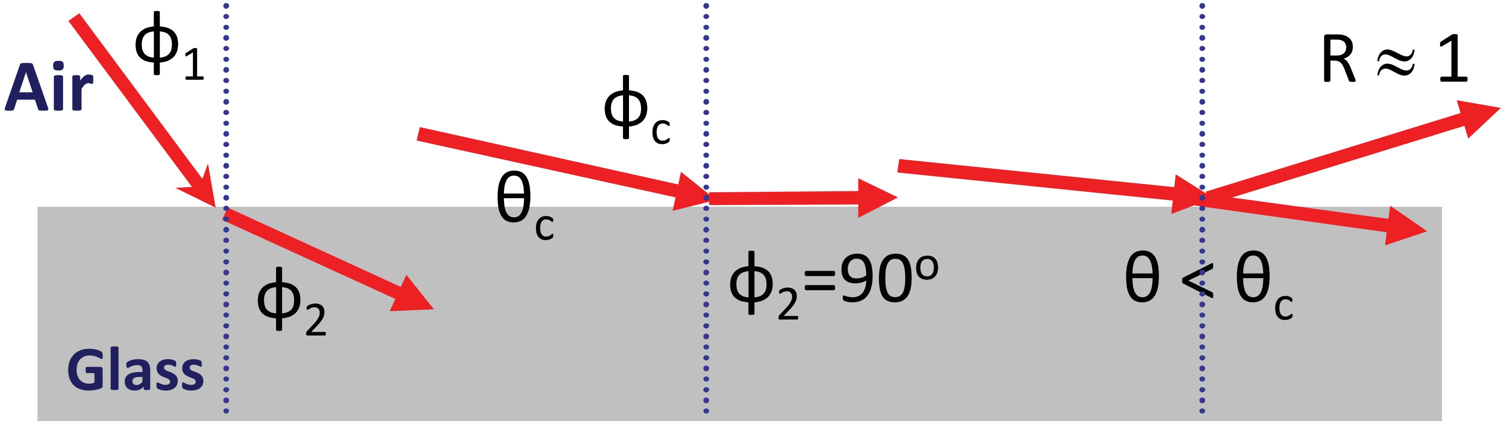

Snell Law: $$\sin\varphi_2 = \frac{\sin\varphi_1}{n} \Rightarrow \varphi_2 > \varphi_1$$

$$\theta_c = \sqrt{2\delta} = \frac{28.8}{E}\cdot\sqrt{\frac{Z_\rho \cdot \rho}{A}}$$

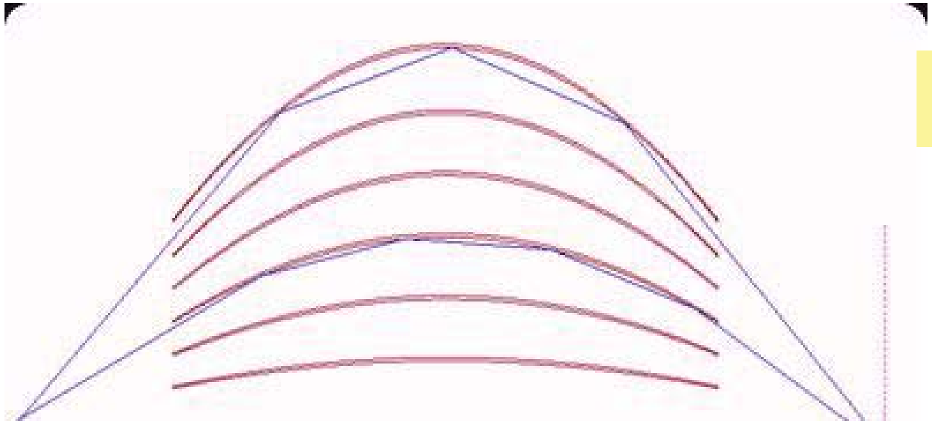

θ_c in the mrad range

Polycapillary X-ray lenses

Bundles of thousands glass mono-capillaries:

- **Directing**
- **Focusing**
- **Parallelizing**

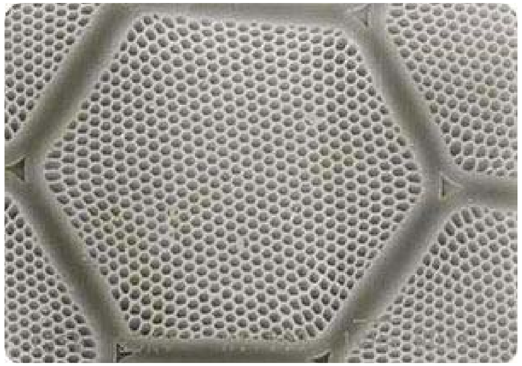

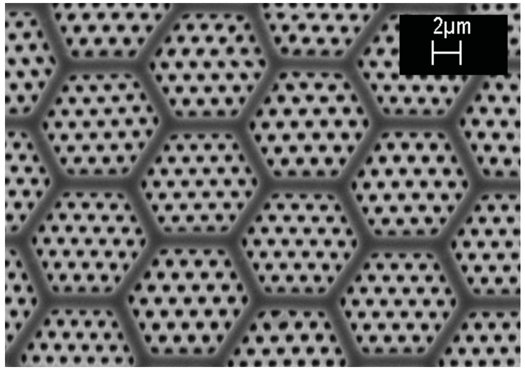

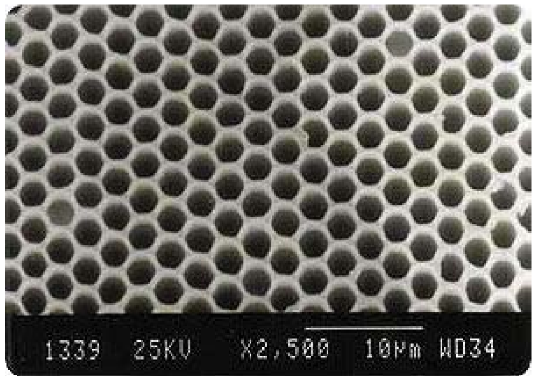

Characteristics of X-Ray lenses

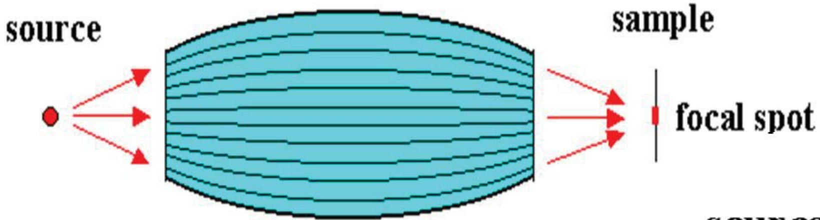

X-ray lens

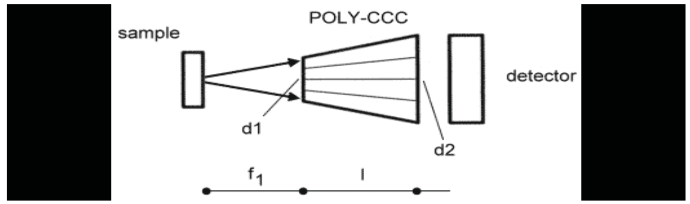

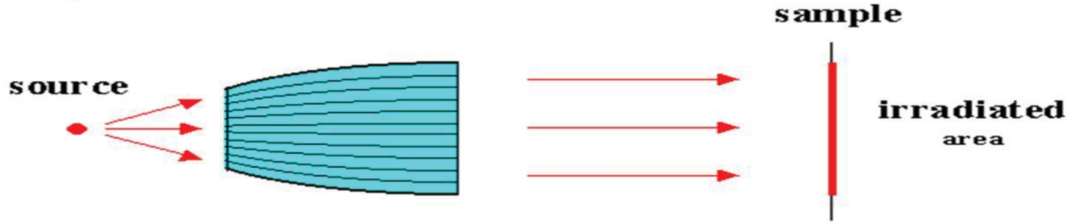

X-ray semilens

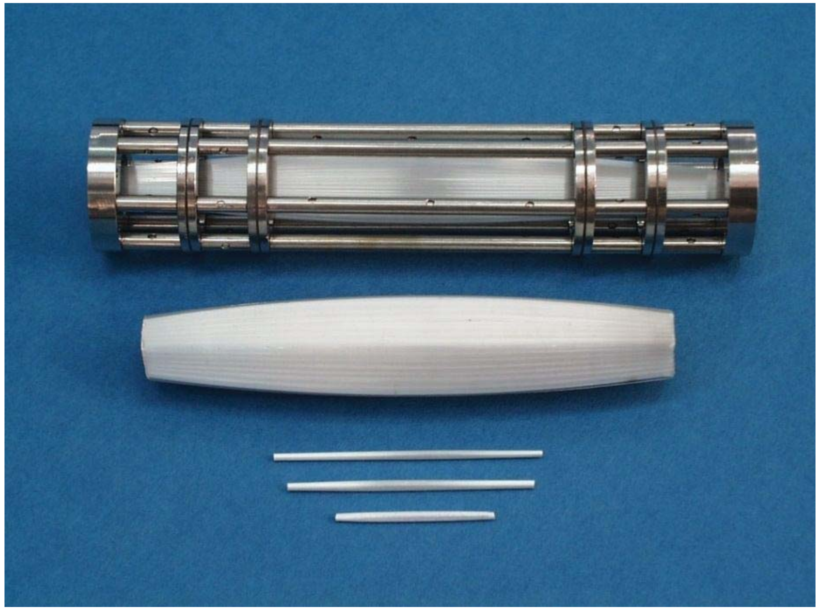

Characteristics of polycappilary X-ray lenses

Important lens parameters:

- **Focal distance** (few mm).
- **Size of the focal region** represented by the FWHM of a Gaussian intensity distribution (down to ~ 12 um @ CuKα)
- ***Transmission efficiency***

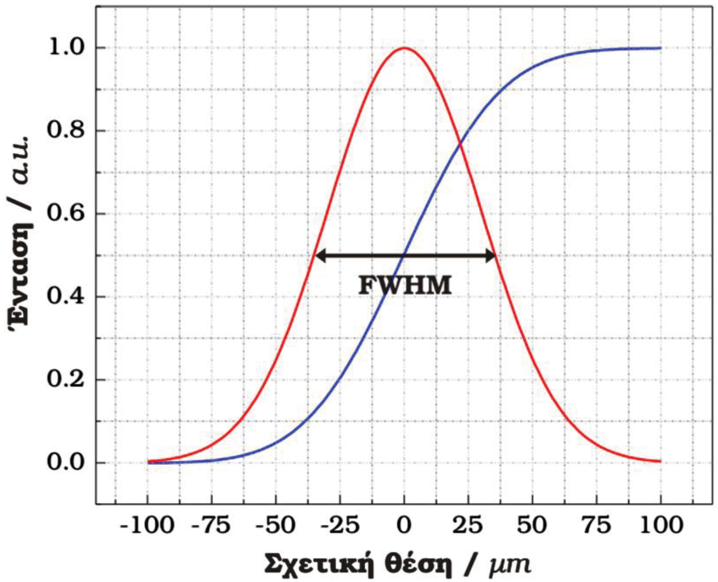

Knife edge scan

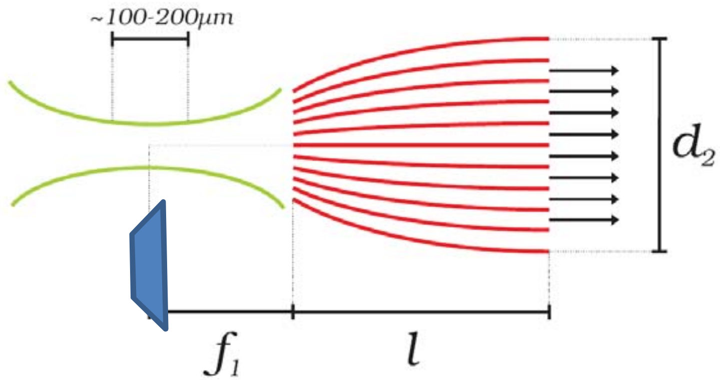

Characteristics of polycappilary X-ray lenses

Nakazawa and Tsuji, XRS, 2013

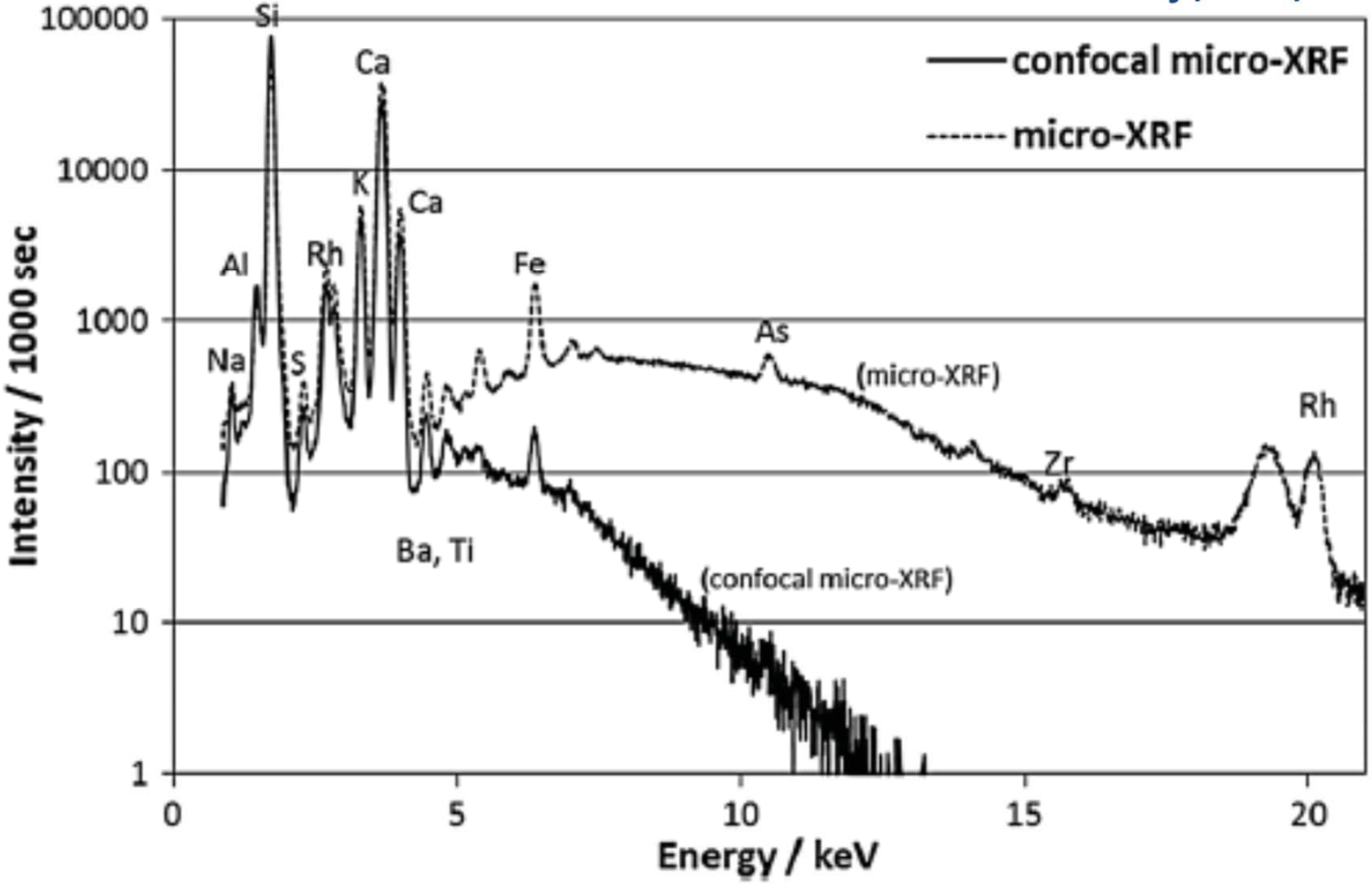

d_2

X-Ray lens spatial resolution

Plane vertical to the optical axis:
Two dimensional Gaussian

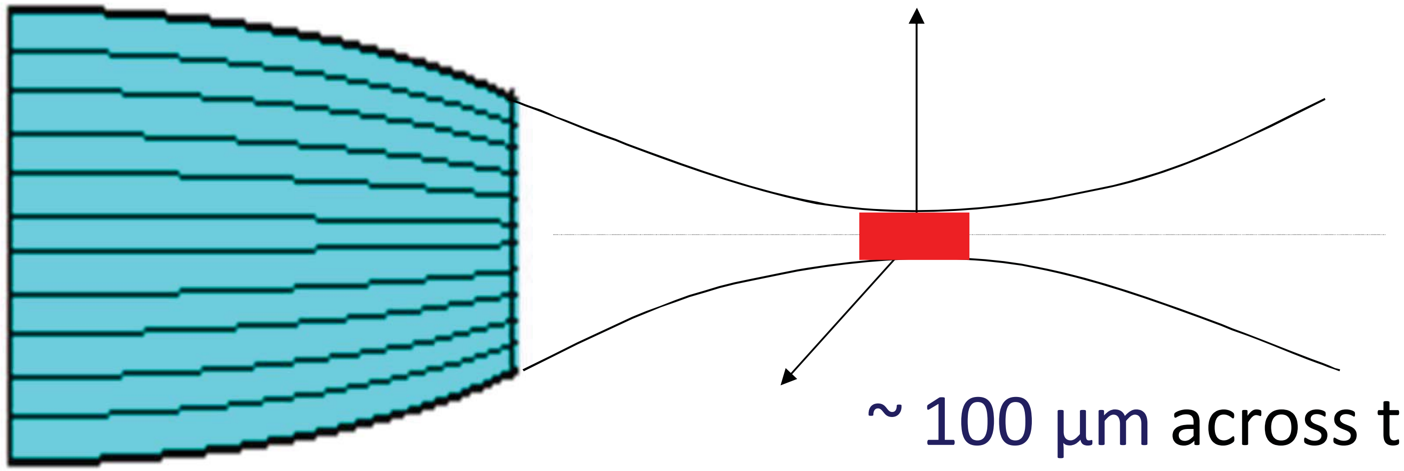

~ 100 μm across the optical axis and the focal plane of the lens the spatial resolution remains constant

PIXE-XRF: Conventional vs Confocal Geometry

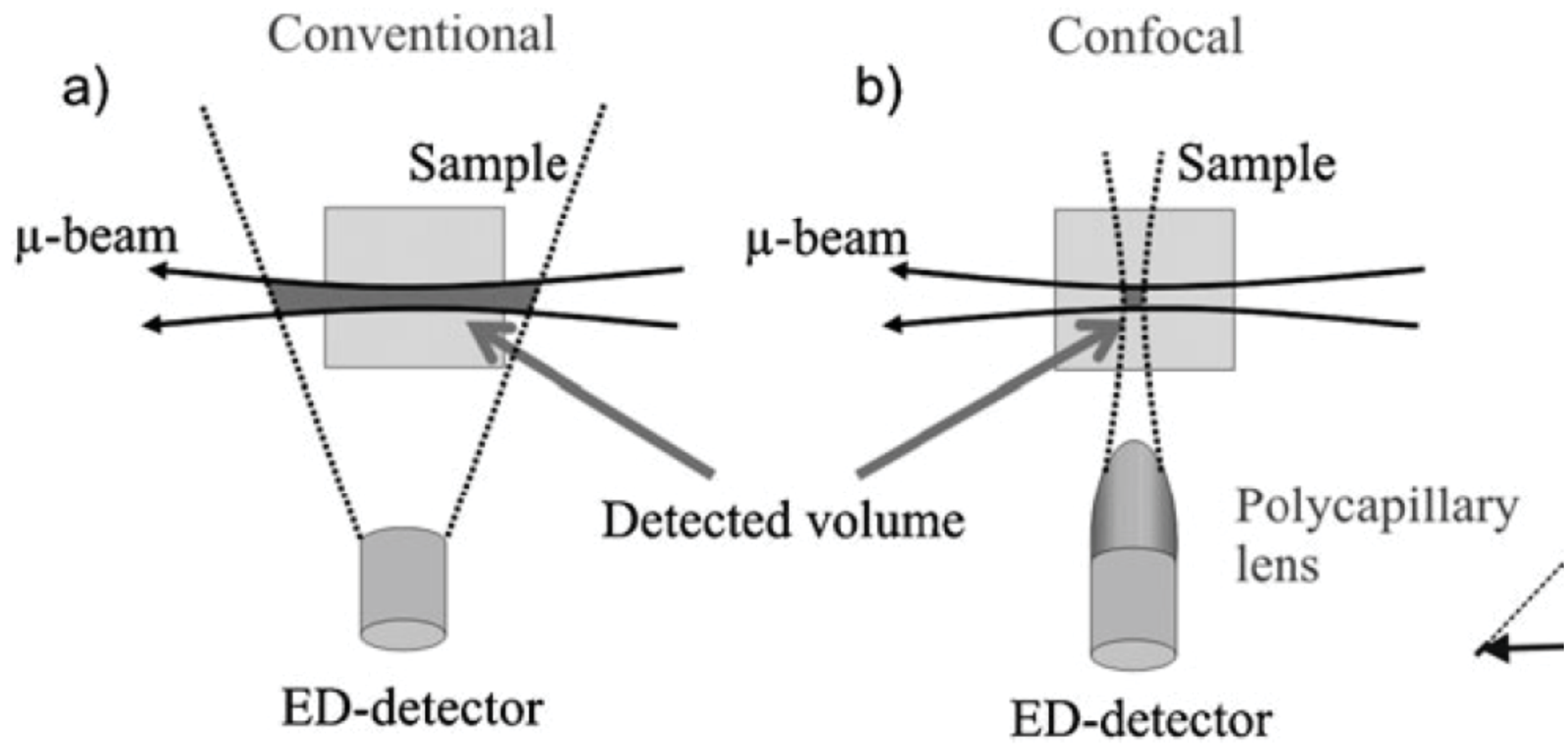

Silversmit et *al*, Phys. Chem. Phys. Chem. 12 (2010) 5653

Principle of Confocal X-ray analysis

B. Kanngießer, I. Reiche, W. Malzer, NIM B 211, 2003

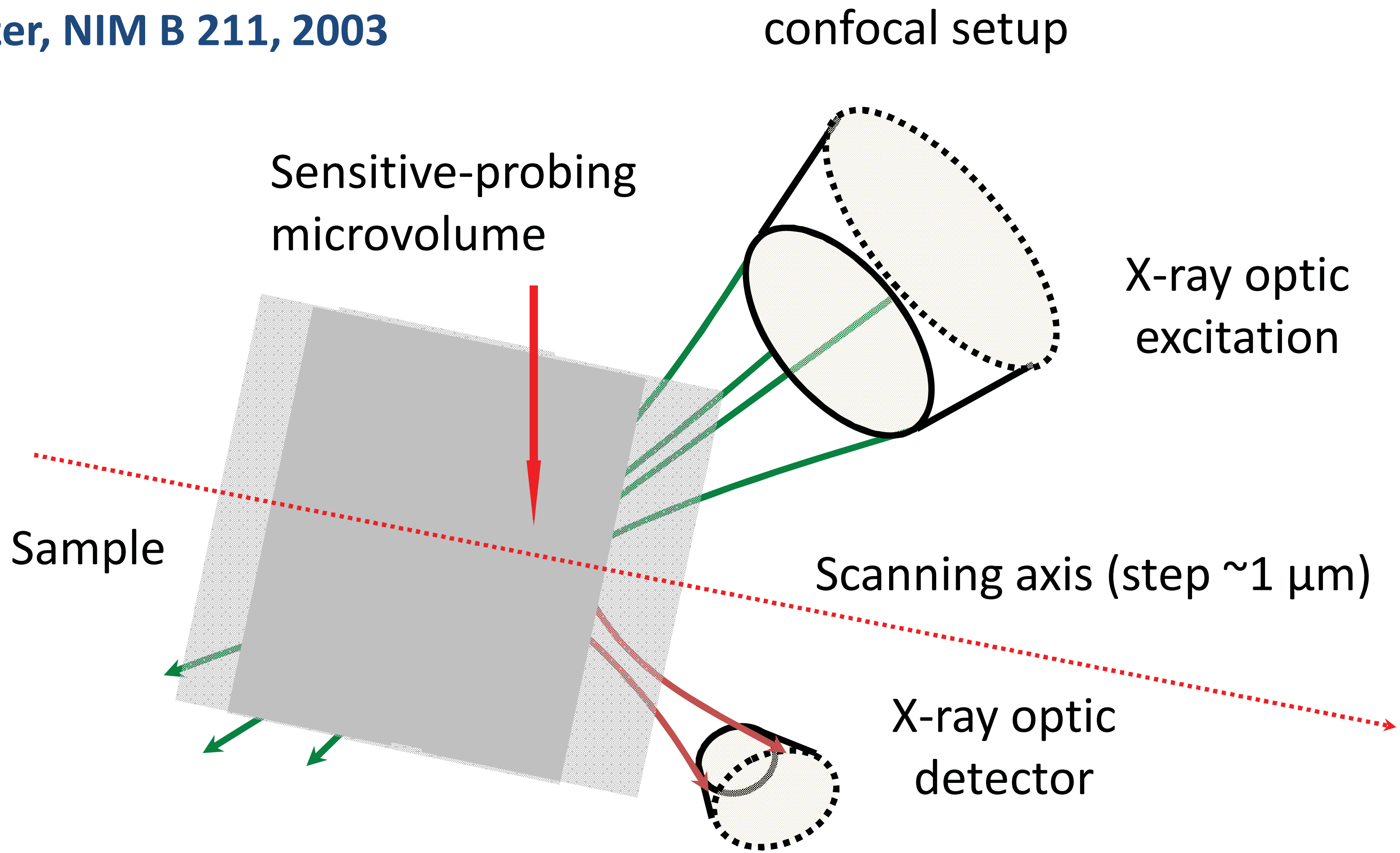

3D Micro XRF Spectrometry:

First setup of the 3D Micro-XRF, @ BAMline, BESSY

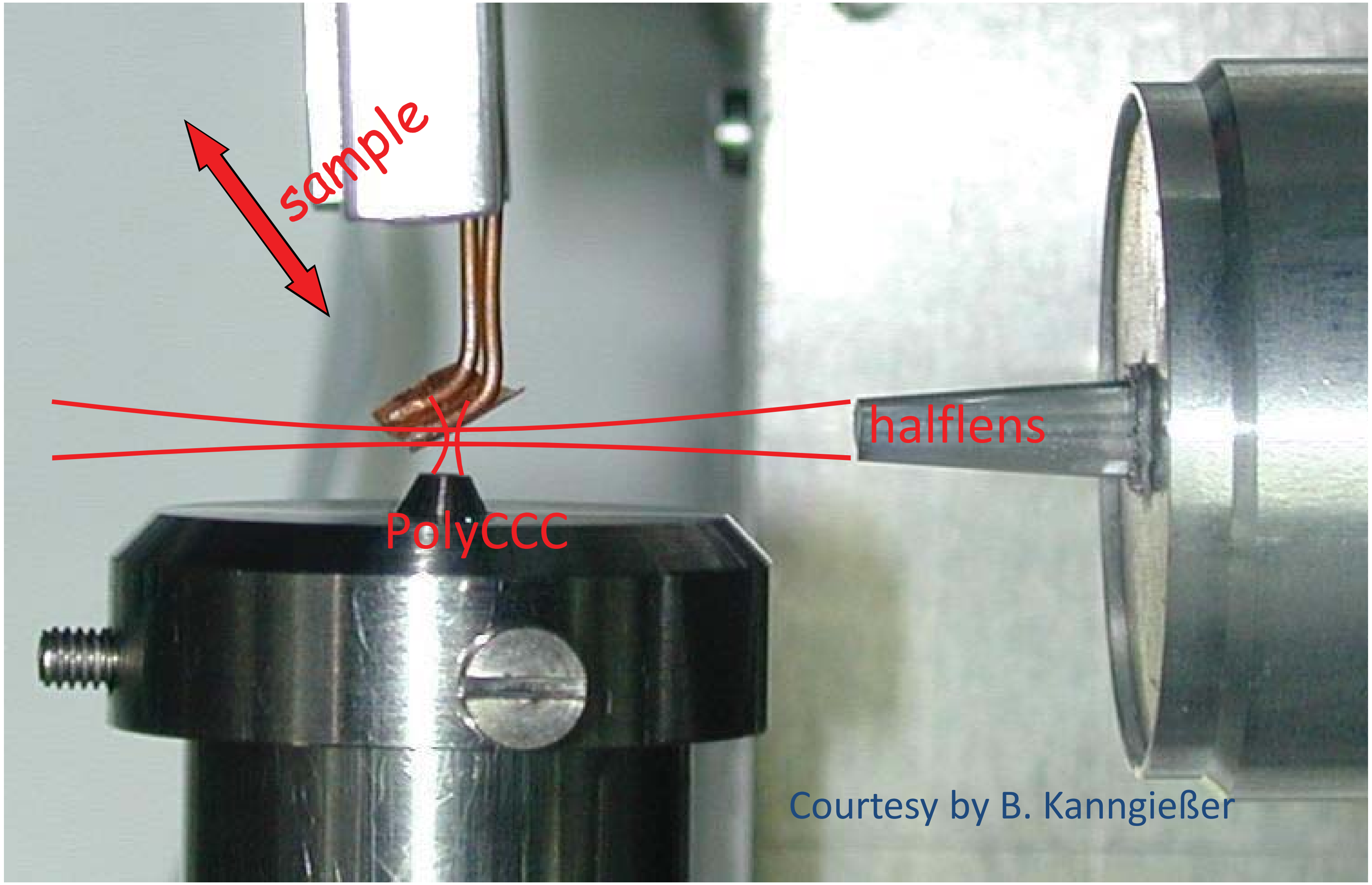

3D Micro–XRF setup: Synchrotron Radiation – μSpot line, BESSY, Berlin

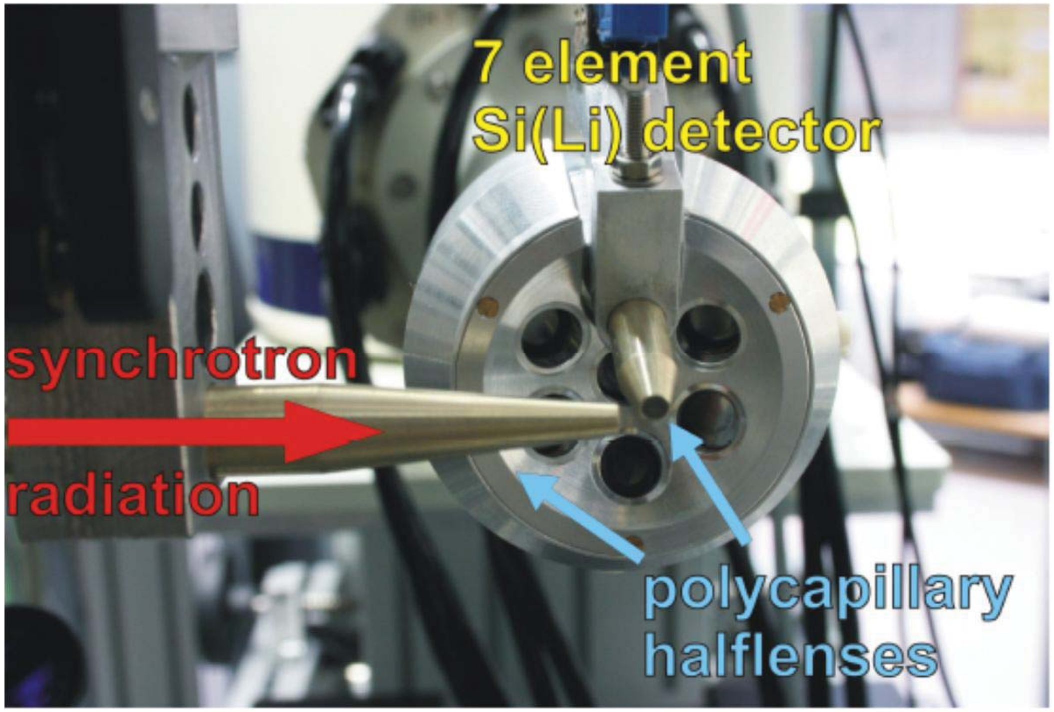

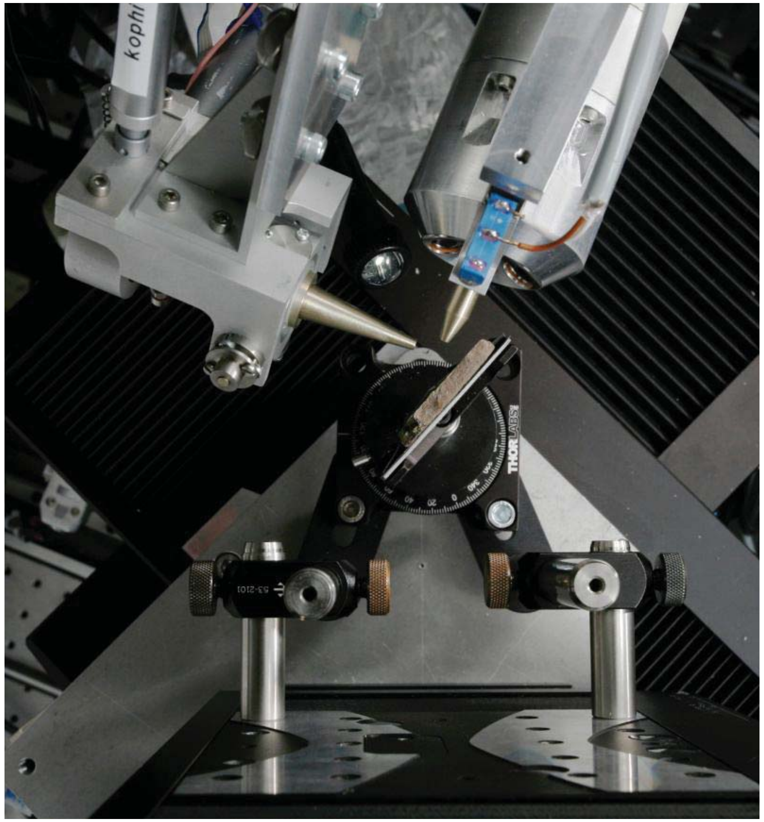

3D Micro–XRF setup @ TU Berlin

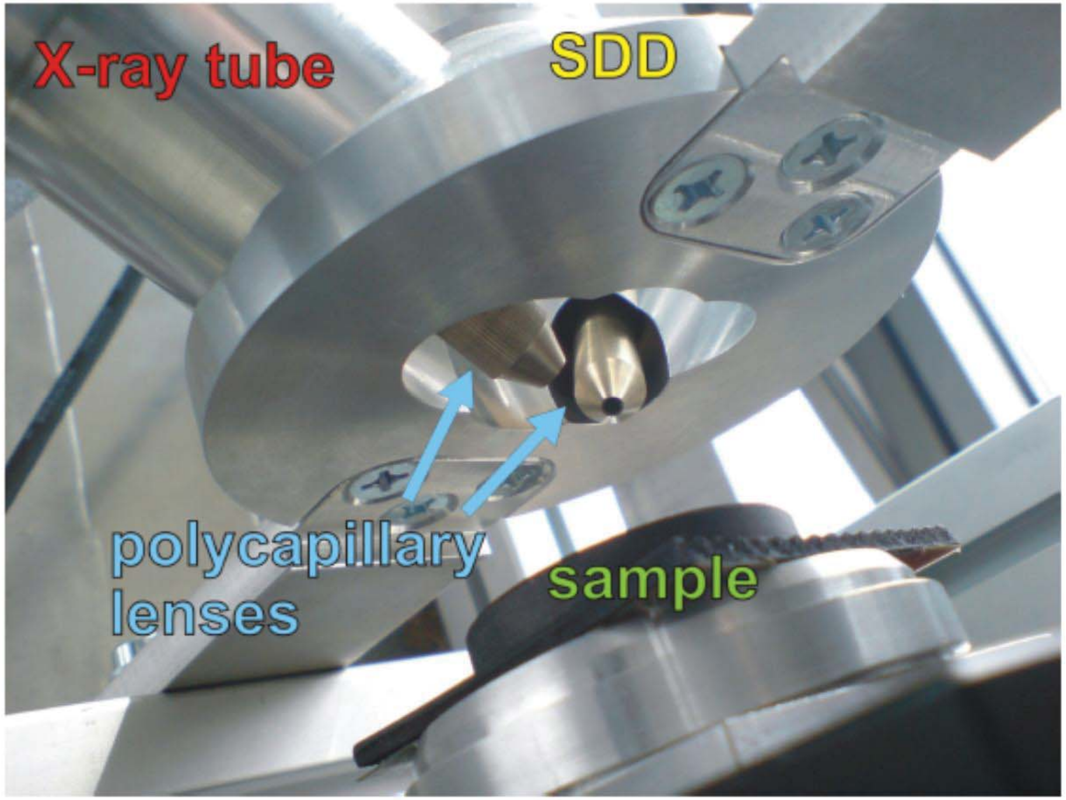

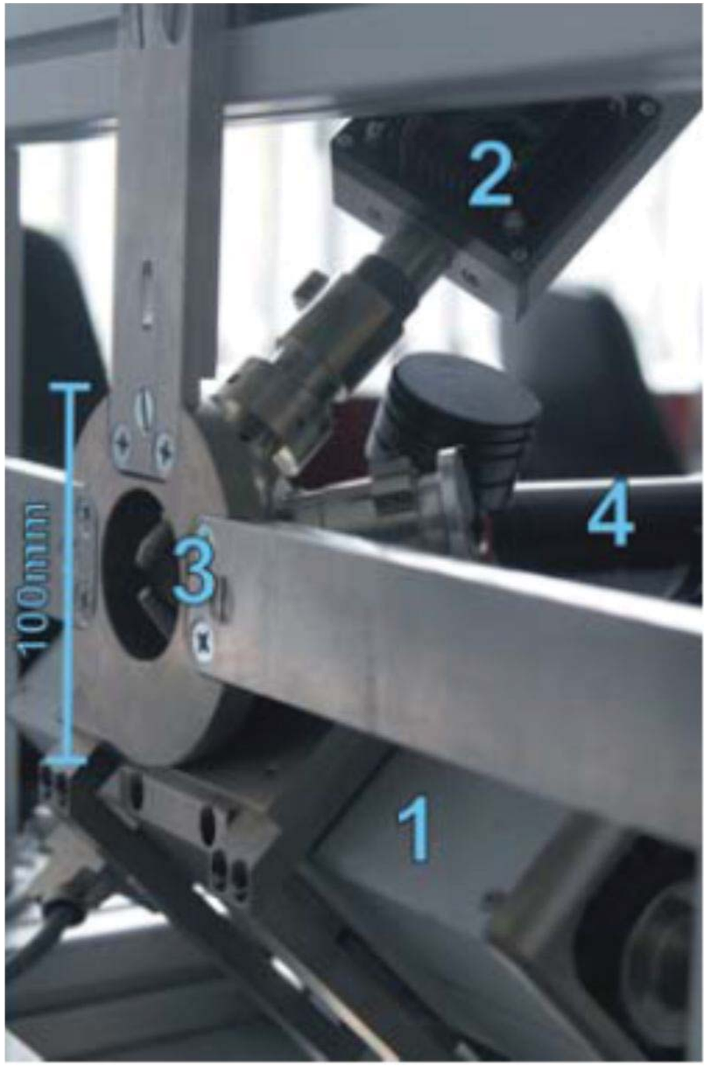

I. Mantouvalou et *al.*, J. Anal. At. Spectrom., 2010, 25, 554–561

Osaka City University, Japan

Tsuji and Nakano, XRS (2007), 36, 145

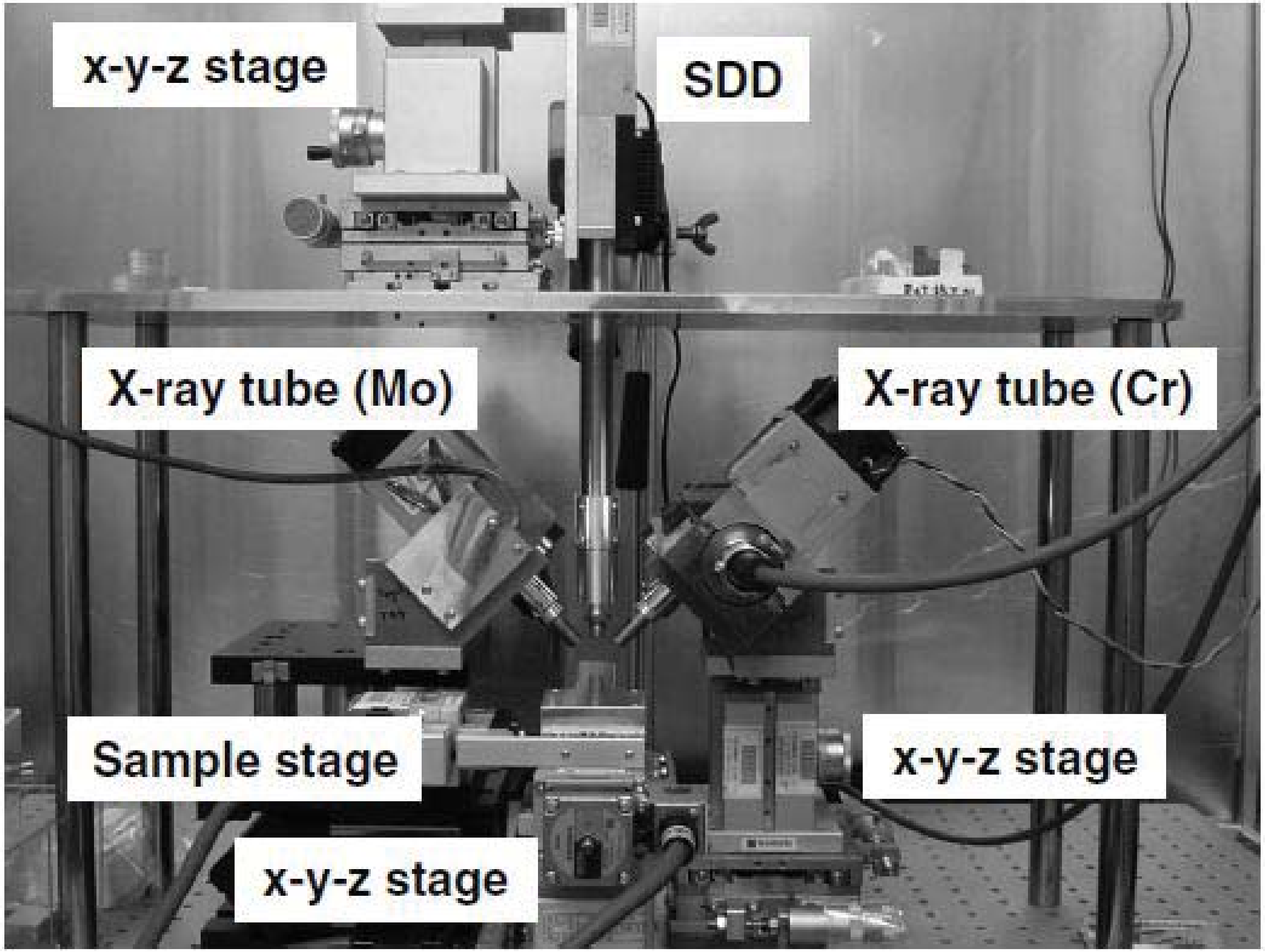

Osaka City University, Japan

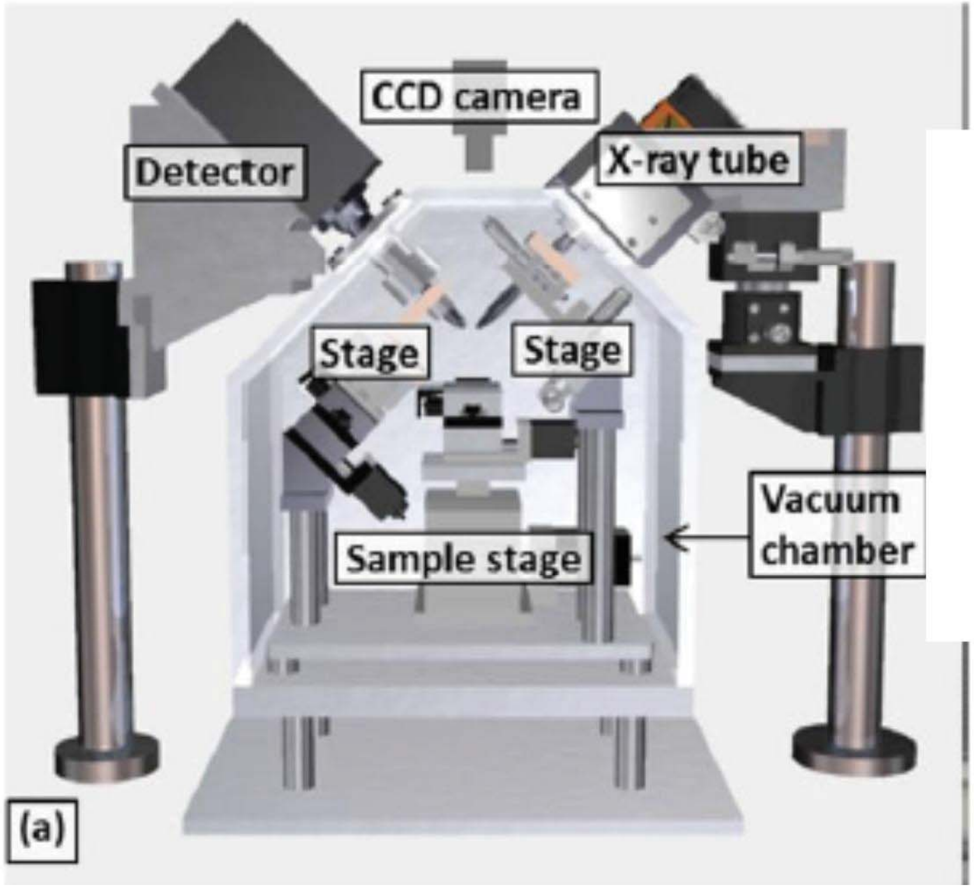

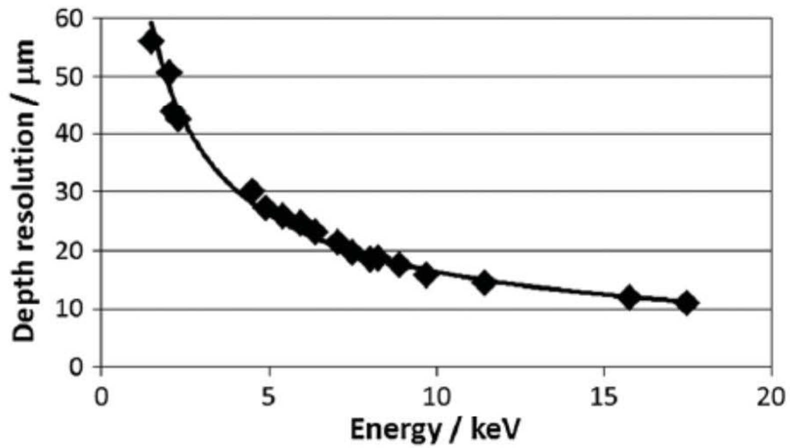

Depth profile for Light elements

Nakazawa and Tsuji, XRS 2013

3D uXRF set-up @IAEA

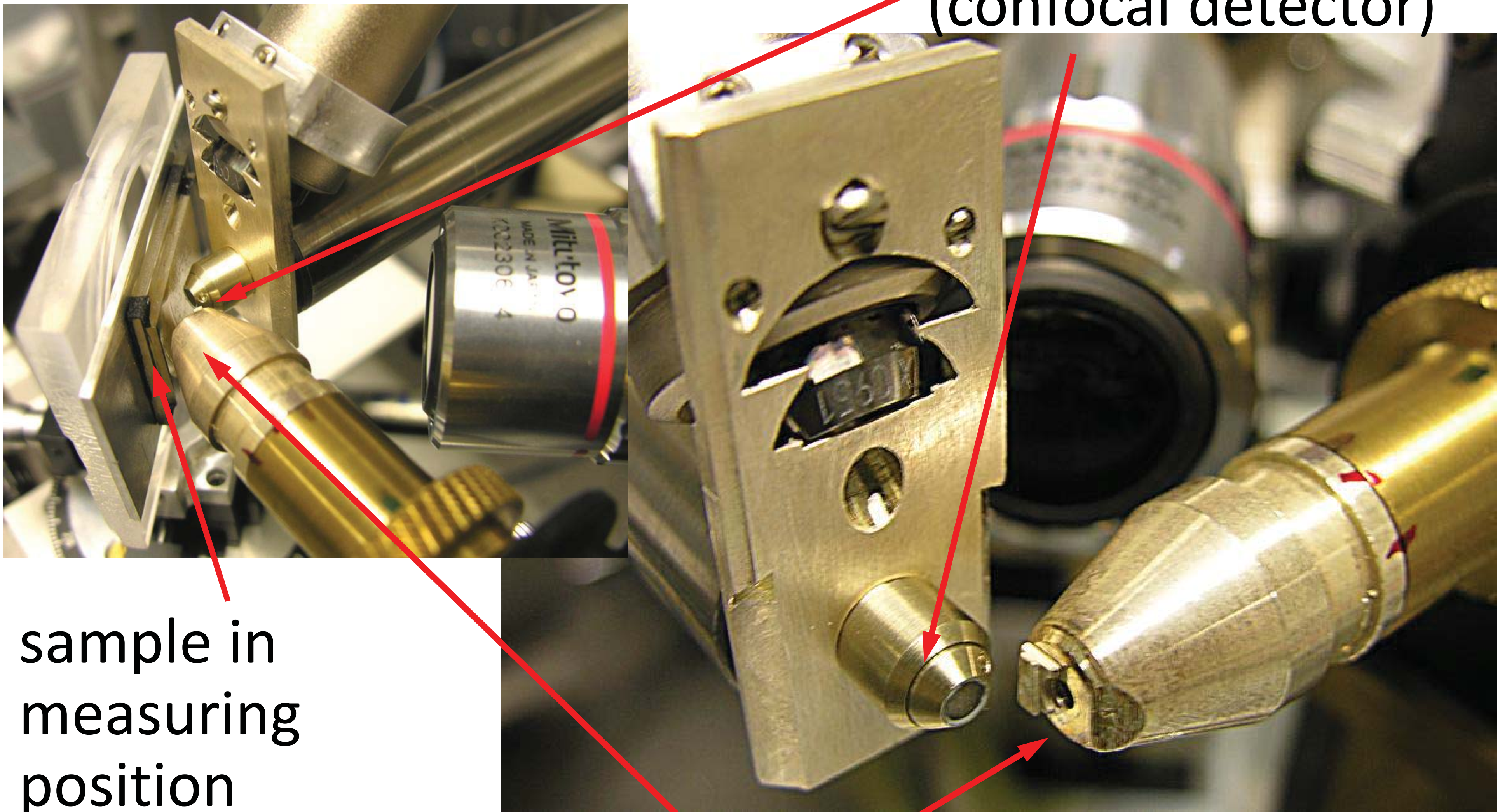

polyCCC
(confocal detector)

sample in
measuring
position

polycapillary (primary beam)

3D Micro-PIXE SET-UP, 2007 @

Josef Stefan Institute Micro-Analytical Center, Ljubljana

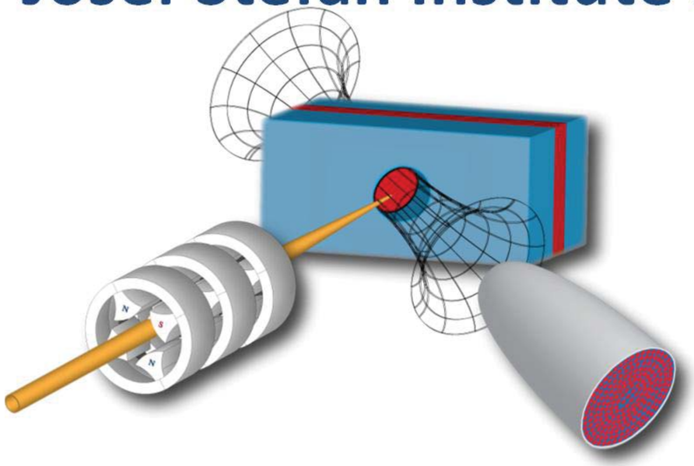

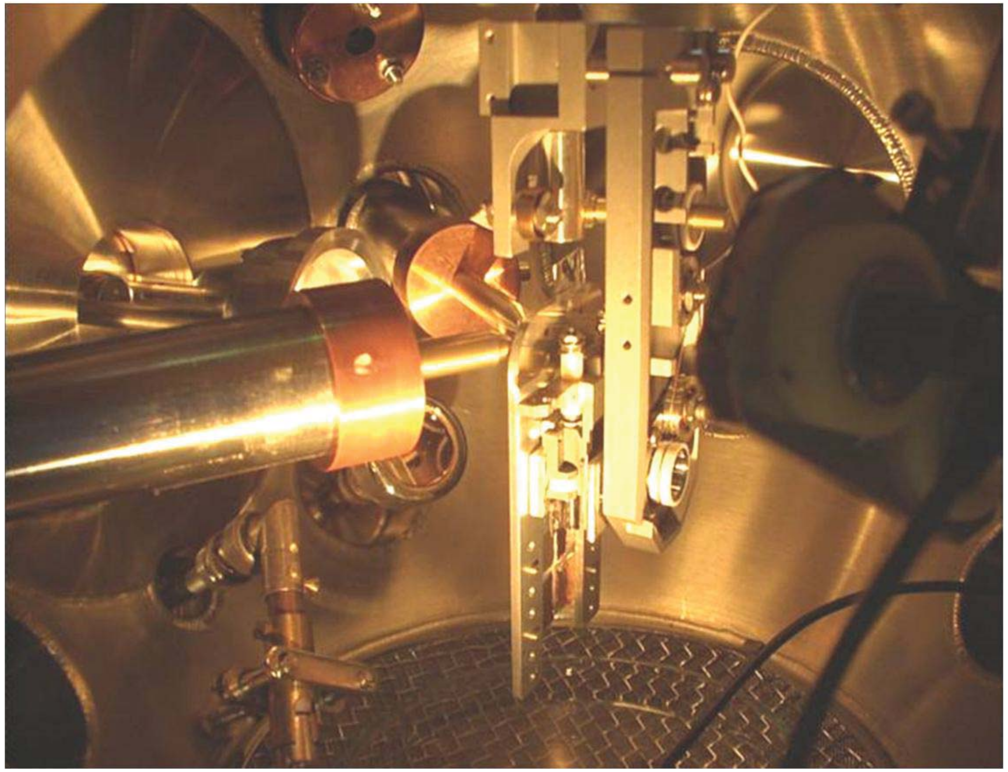

Karydas et al, JAAS 2007

Basics in XRF Quantification

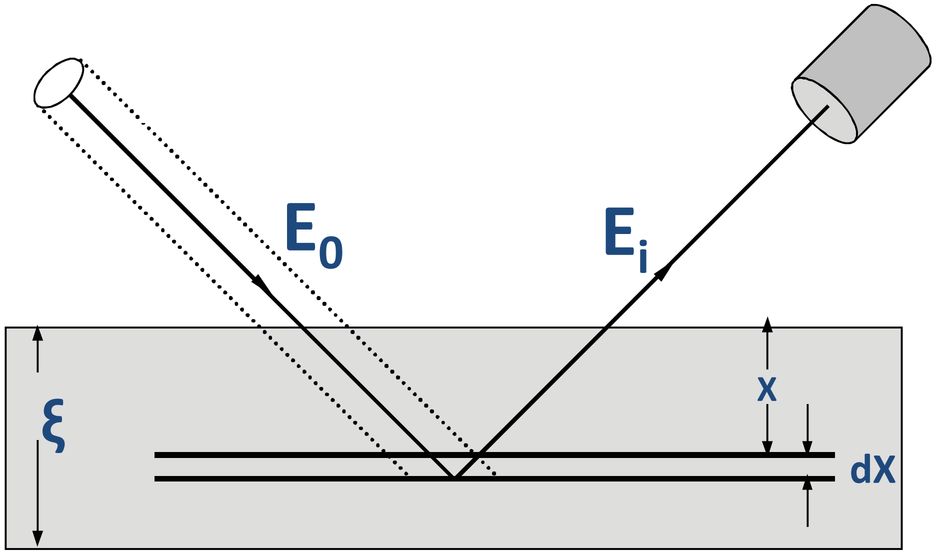

- ✓Monochromatic excitation
- ✓Homogeneous sample

$$\mu_s(E_o, E_i) = \sum_{k=1}^{n} c_k \cdot \left[\frac{\mu_k(E_0)}{\sin\theta_1} + \frac{\mu_k(E_i)}{\sin\theta_2} \right]$$

$$I_a(E_i) = I_o \cdot G \cdot \sigma_i^a(E_0) \cdot f_{ab}(E_i) \cdot \varepsilon_d(E_i) \cdot c_a \cdot \frac{1 - \exp\left[-\mu_s(E_o, E_i)\cdot\xi\right]}{\mu_s(E_i)}$$

Geometrical Factor

Detector Efficiency

Beam Intensity

Cross section

Air absorption

Analyte Concentration

Sensitivity constant

IAEA

A.G. Karydas, Joint ICTP-IAEA workshop, April 22-26, 2013

Quantification in Confocal Micro XRF (1)

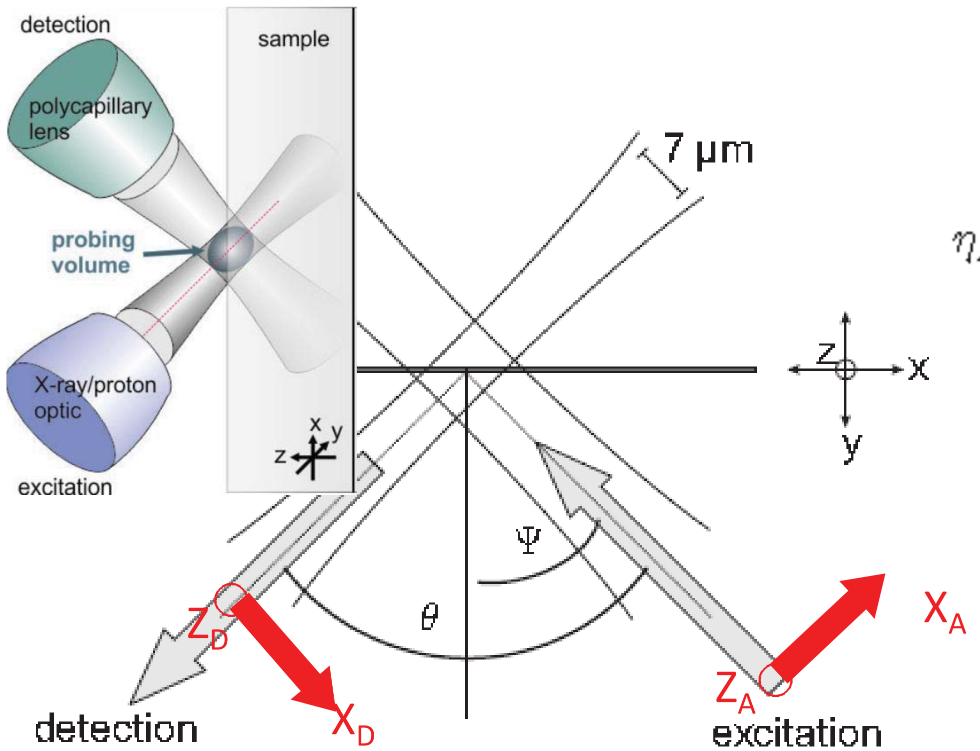

Intensity distribution for the exciting x-ray beam:

$$\eta_A = \frac{T_A}{2\pi\sigma_A^2}\exp\left(-\frac{x_A^2+z_A^2}{2\sigma_A^2}\right)$$

Coordination system attached to the excitation lens

T_A, T_B: Lens transmission

σ_A, σ_B : Spot size

Ω **:** solid angle

$$\eta_D = \frac{\Omega T_D}{4\pi}\exp\left(-\frac{x_D^2+z_D^2}{2\sigma_D^2}\right)$$

Coordination system attached to the detection lens

3D set-up sensitivity for the detection of specific fluorescence lines

The shape has a three dimensional **ellipsoid**

$$\begin{aligned}\hat{\eta}(x,y,z) &= \eta_A\eta_D\epsilon \\ &= \frac{\Omega T_A T_D \epsilon}{8\pi^2\sigma_A^2}\exp\left(-\frac{\sigma_D^2 x_A^2+\sigma_A^2 x_D^2+(\sigma_D^2+\sigma_A^2)z^2}{2\sigma_A^2\sigma_D^2}\right)\end{aligned}$$

Quantification in Confocal Micro XRF (2)

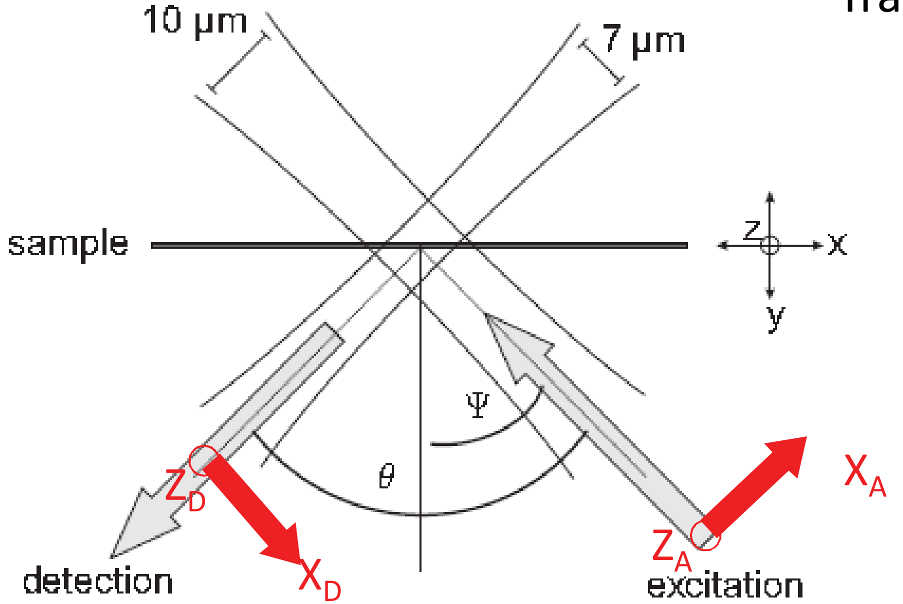

Transformation to the sample coordinate system

$$x_A = x\sin(\Psi) + y\cos(\Psi)$$
$$x_D = x\cos(\Psi) - y\sin\Psi$$
$$z_A = z_D = z$$

$$\tilde{\eta}(y) = \int_{-\infty}^{\infty}\int_{-\infty}^{\infty}\hat{\eta}(x,y,z)dxdz$$

$$= \frac{\Omega T_A T_D \epsilon}{4\pi}\frac{\sigma_D^2}{\sqrt{(\sigma_D^2+\sigma_A^2)(\cos^2(\Psi)\sigma_A^2+\sin^2(\Psi)\sigma_D^2)}}\exp\left(-\frac{1}{2}\frac{y^2}{(\sin^2(\Psi)\sigma_D^2+\cos^2(\Psi)\sigma_A^2)}\right)$$

Mantouvalou, PhD Thesis, Berlin 2009
Maltzer, kanngiesser, SAB 60 (2005) 1334 – 1341

$$= \frac{\eta}{\sqrt{2\pi}\sigma_y}\exp\left(-\frac{y^2}{2\sigma_y^2}\right)$$

Quantification in Confocal Micro XRF (3)

Fluorescence intensity in confocal geometry for an homogeneous sample

$$\Phi_i(y) = \Phi_o \cdot \sigma_{F.i} \int_o^D \overline{\eta}_i(\zeta - y)\,\rho_i(\zeta) \cdot \exp(-\overline{\mu}_{lin,i}\zeta) \cdot d\zeta$$

Local density of element *i*

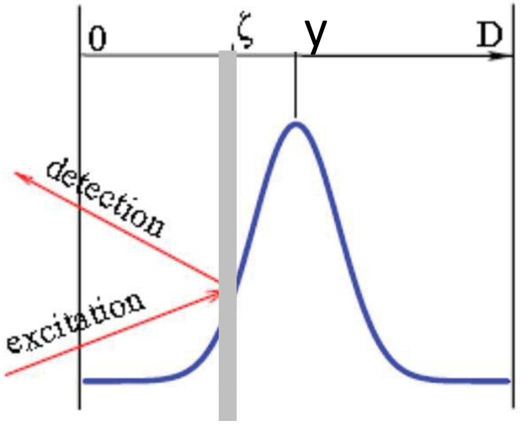

$$\bar{\mu}_{lin,i} = \bar{\mu}_i \cdot \rho = \left(\sum_{elements\ j} \left(\frac{\mu_{0,j}}{\cos(\theta_A)} + \frac{\mu_{i,j}}{\cos(\theta_D)} \right) w_j \right) \rho$$

$$= \sum_{elements\ j} \left(\frac{\mu_{0,j}}{\cos(\theta_A)} + \frac{\mu_{i,j}}{\cos(\theta_D)} \right) \rho_j$$

$$\Phi_i(y) = \frac{\Phi_o \cdot \eta_i \cdot \rho_i \cdot \sigma_{F.i}}{2} \times \exp\left(\frac{(\overline{\mu}_{lin,i}\sigma_{y,i})^2}{2} \right) \times \exp(-\overline{\mu}_{lin,i}\, y) \times$$

$$\times \left[erf\left(\frac{D + \overline{\mu}_{lin,i}\sigma_{y,i}^2 - y}{\sqrt{2}\sigma_{y,i}} \right) - erf\left(\frac{\overline{\mu}_{lin,i}\sigma_{y,i}^2 - y}{\sqrt{2}\sigma_{y,i}} \right) \right]_i$$

corrects for the actual extension of the probing volume

stands for the decrease of the intensity at probing depth x due to absorption.

important if the probing volume intersects the layer boundaries.

Shape of intensity profiles versus depth

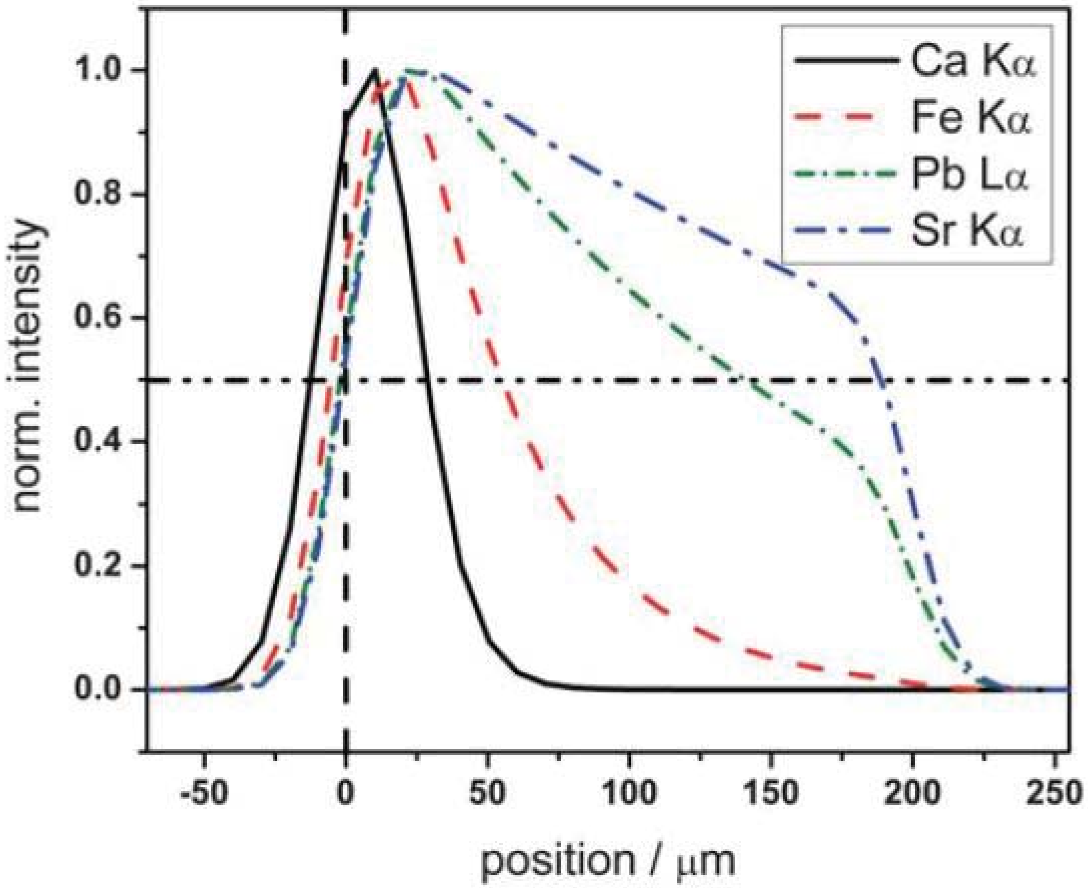

SiO_2 matrix, similar concentration (50 ppm), 19 keV excitation

I. Mantouvalou et *al.*, J. Anal. At. Spectrom., 2010, 25, 554–561

Experimental FWHM, sensitivity/3D uXRF

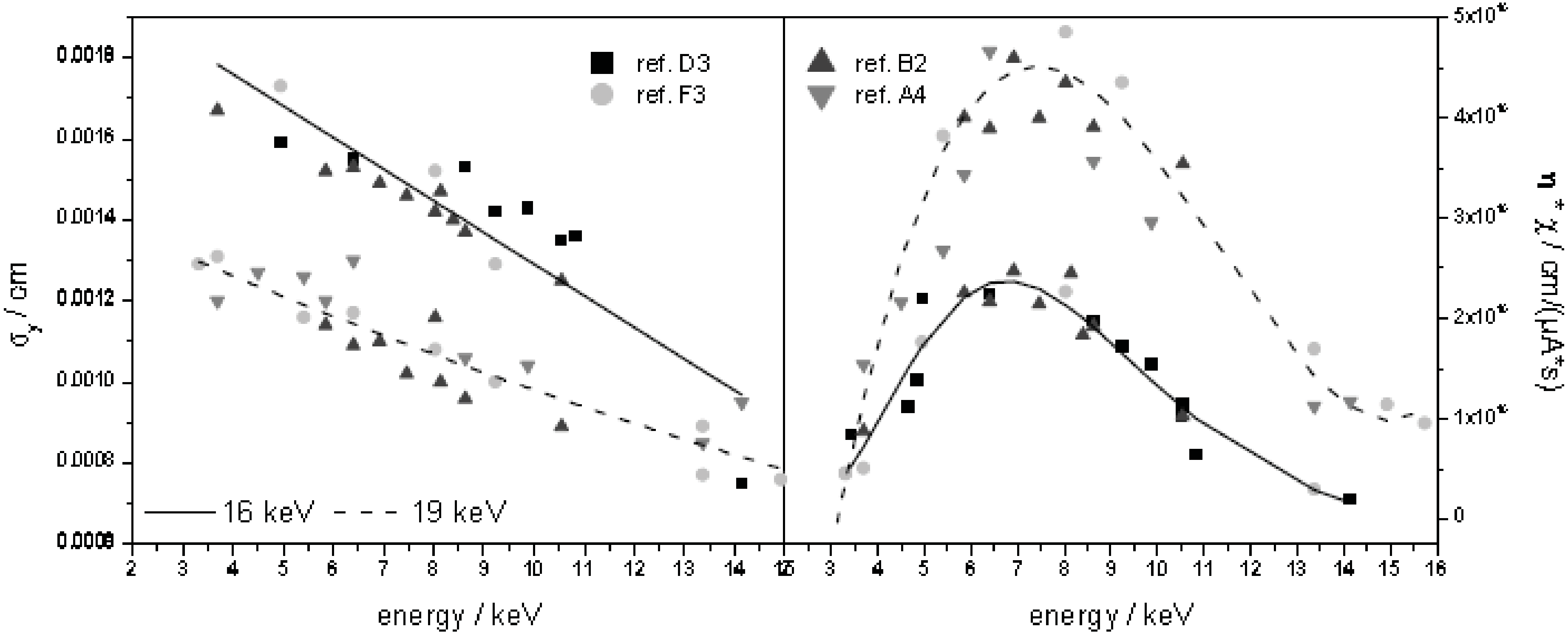

16, 19 keV excitation energies, Glass Reference materials

I. Mantouvalou, PhD Thesis, Berlin 2009

First 3D Micro-XRF application:
Indian Mughal-Paintings 16th – 18th century

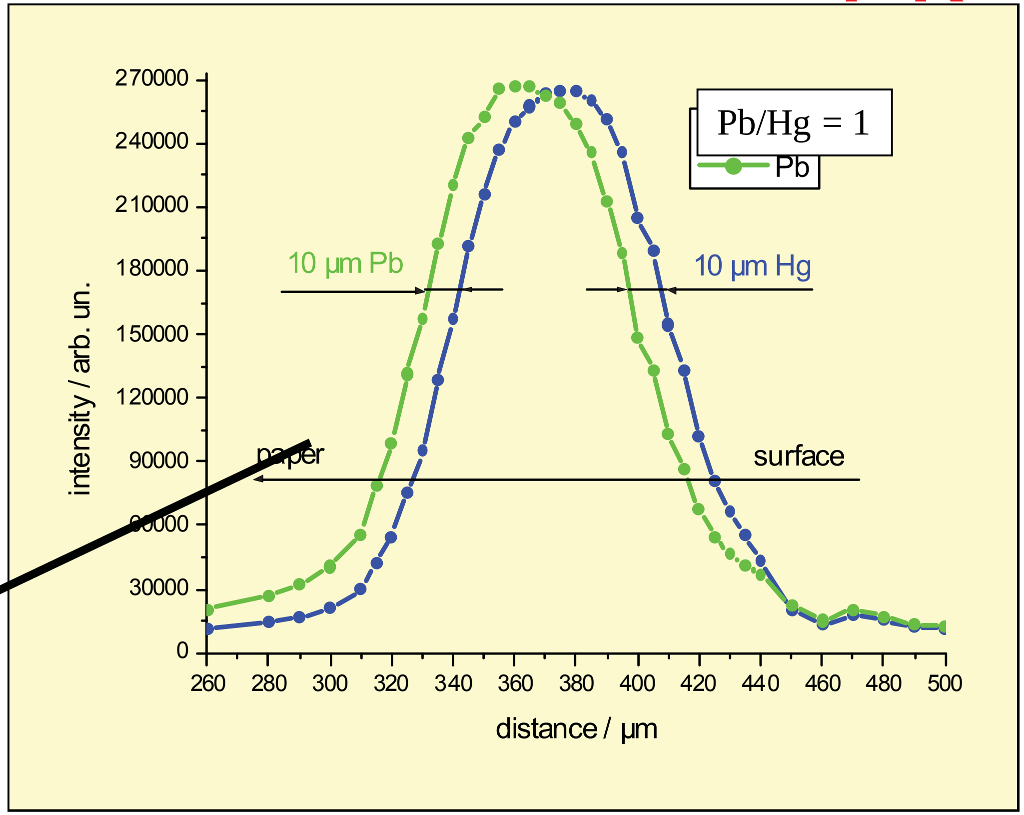

B. Kanngießer, I. Reiche, W. Malzer,
NIM B 211, 2003

3D uXRF for Paint layers

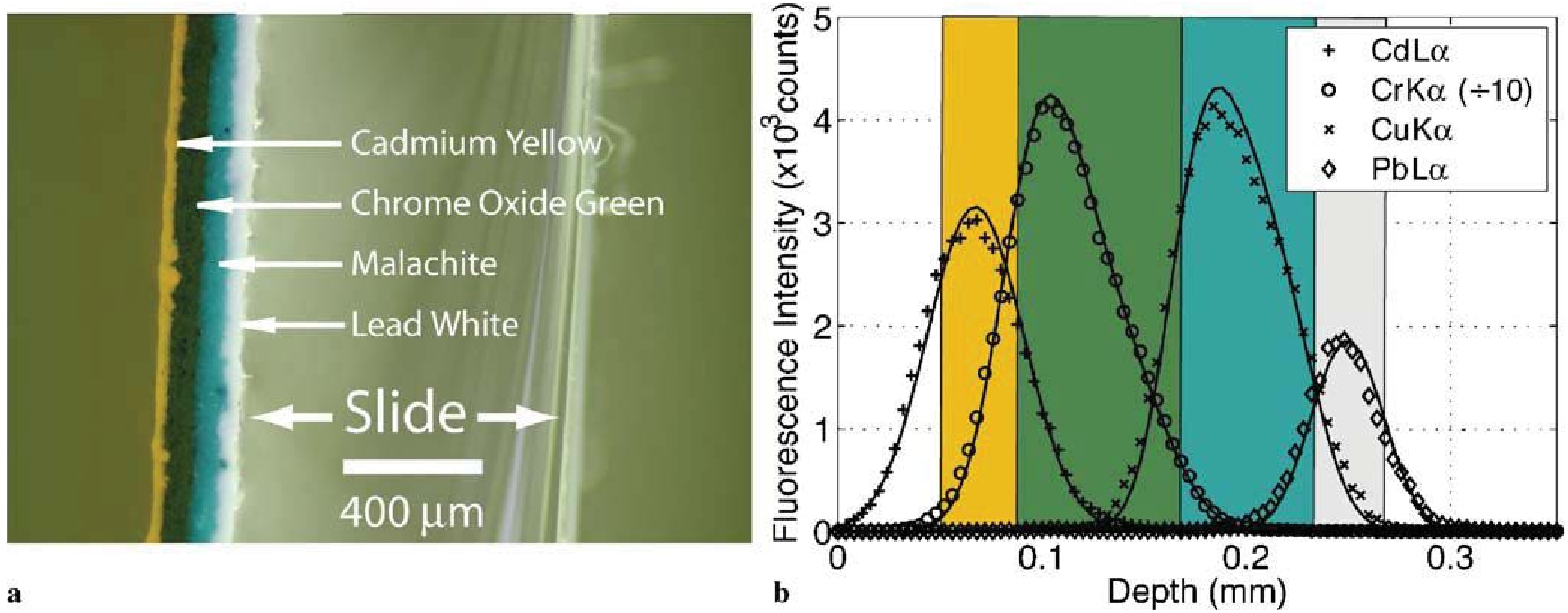

Woll et *al* Appl. Phys. A 83, 235–238 (2006)

3D Micro-PIXE applications:
Multilayered sample

Artificially prepared multilayer structure

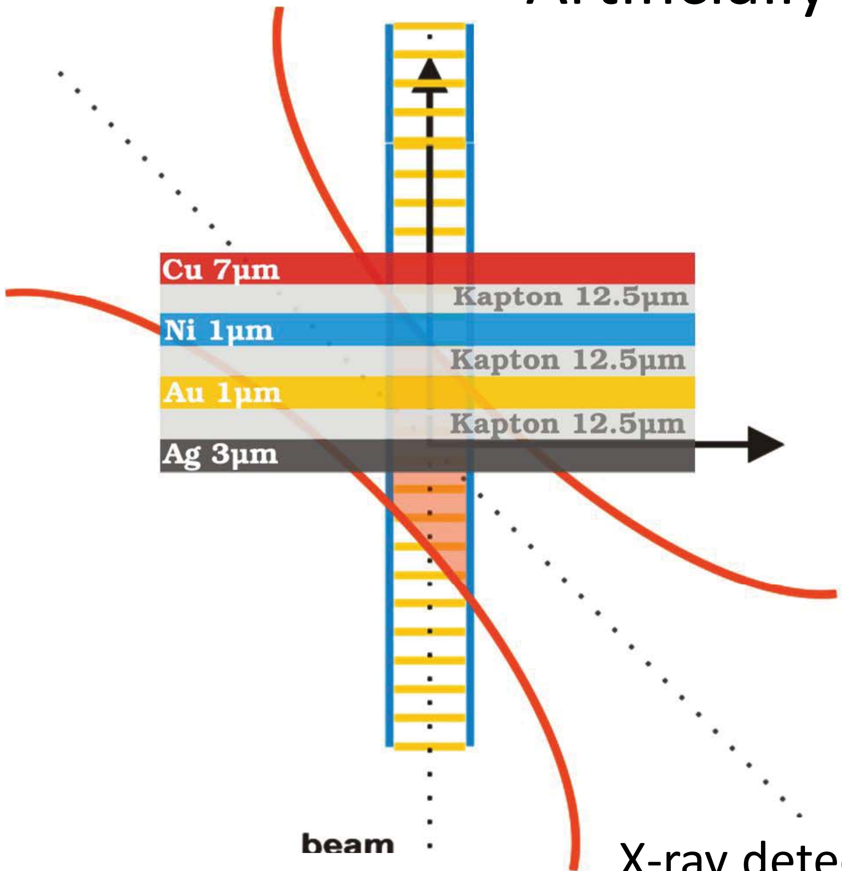

Microbeam

X-ray detector

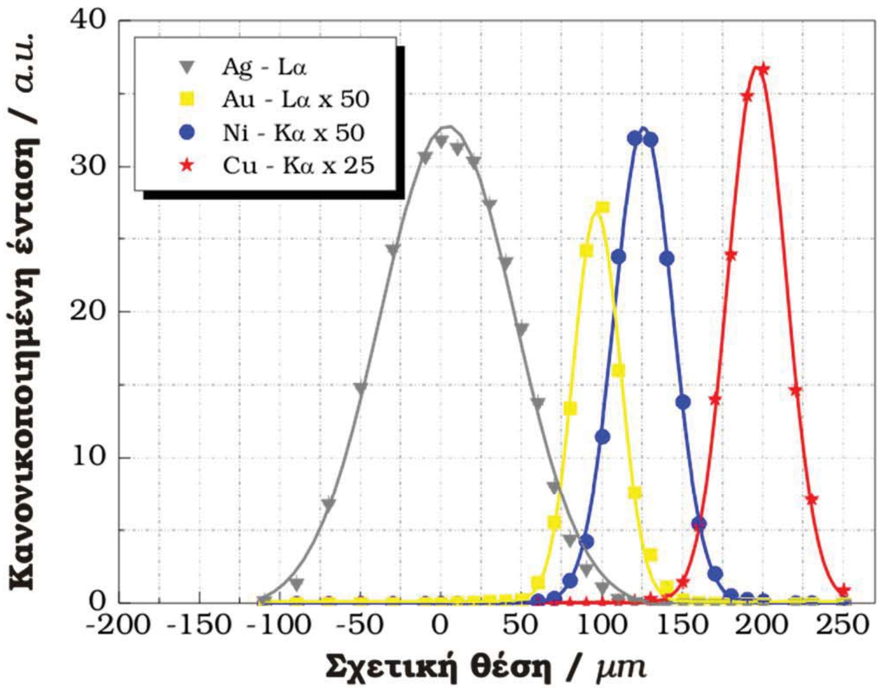

A.G. Karydas, et al, J. Anal. At. Spectrom., 2007

3D Micro-PIXE: First applications

PIXE spectra for two different positions of the sample within the sensitive probing-microvolume

Artificially prepared multilayer structure

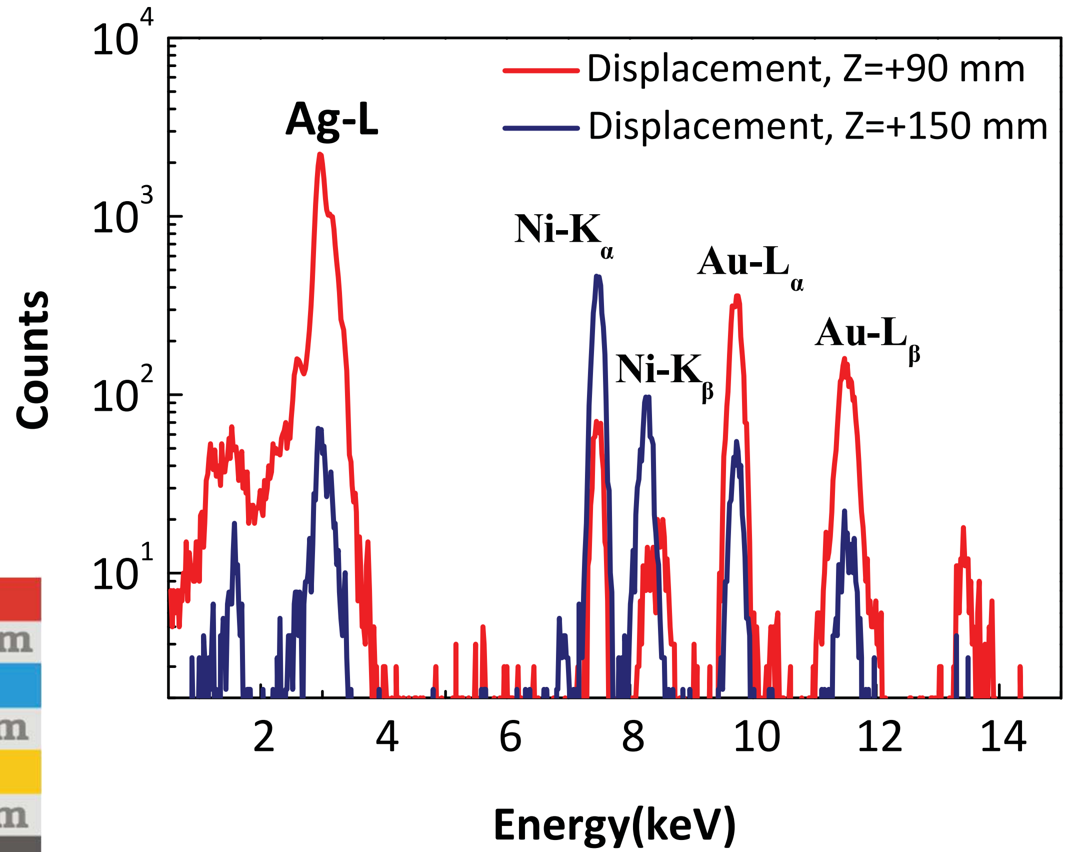

Methodology development: Quantification in 3D Micro-XRF using X-ray tube excitation

S4:
Multilayer
Polymer
sample
doped with
Fe and Cu

Fe/Cu/Fe/Cu/Fe/Cu/Fe/Cu/Fe

Intensity profiles versus depth

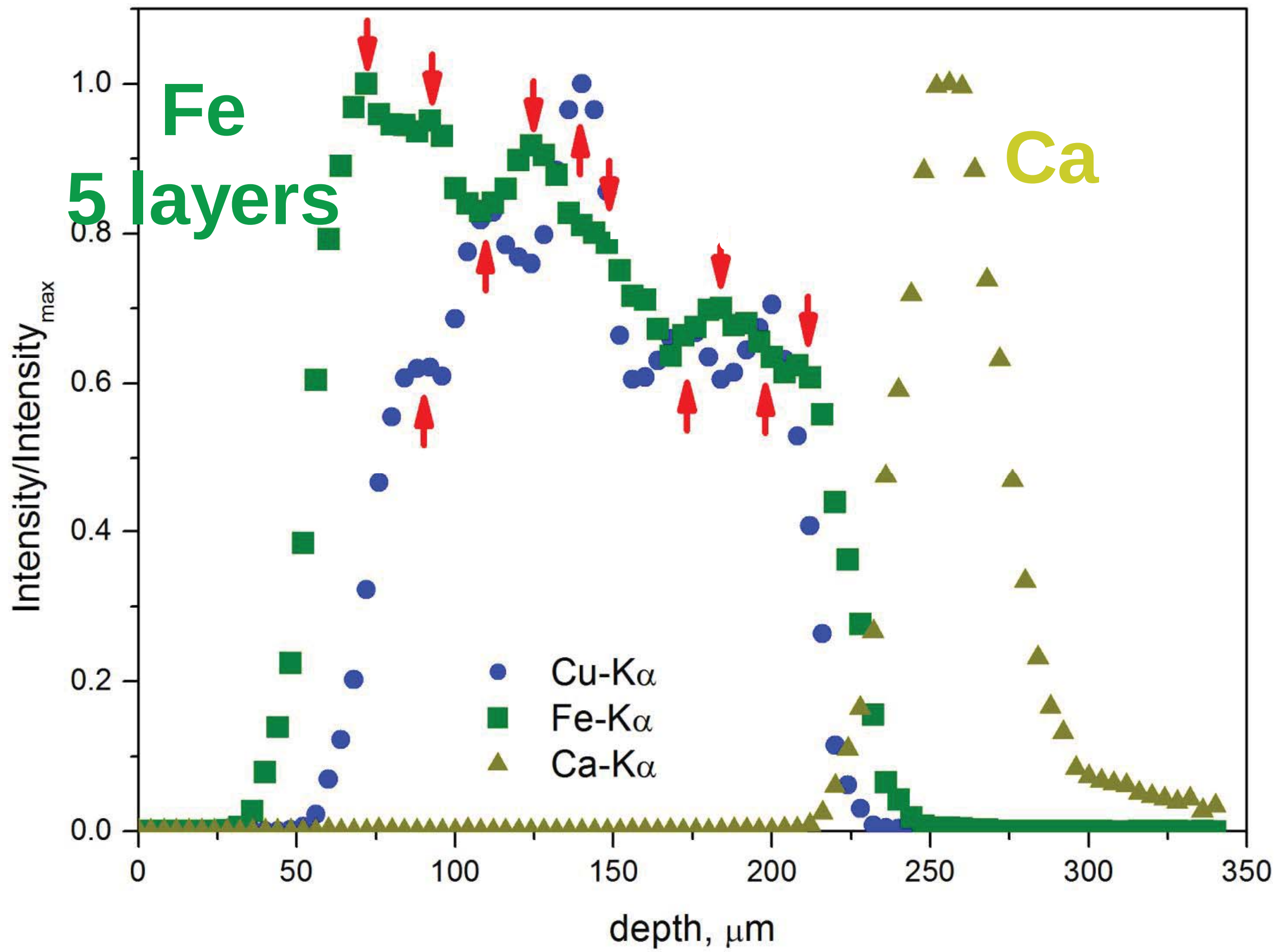

Average of 10 depths cans

3D Imaging of raw intensity data

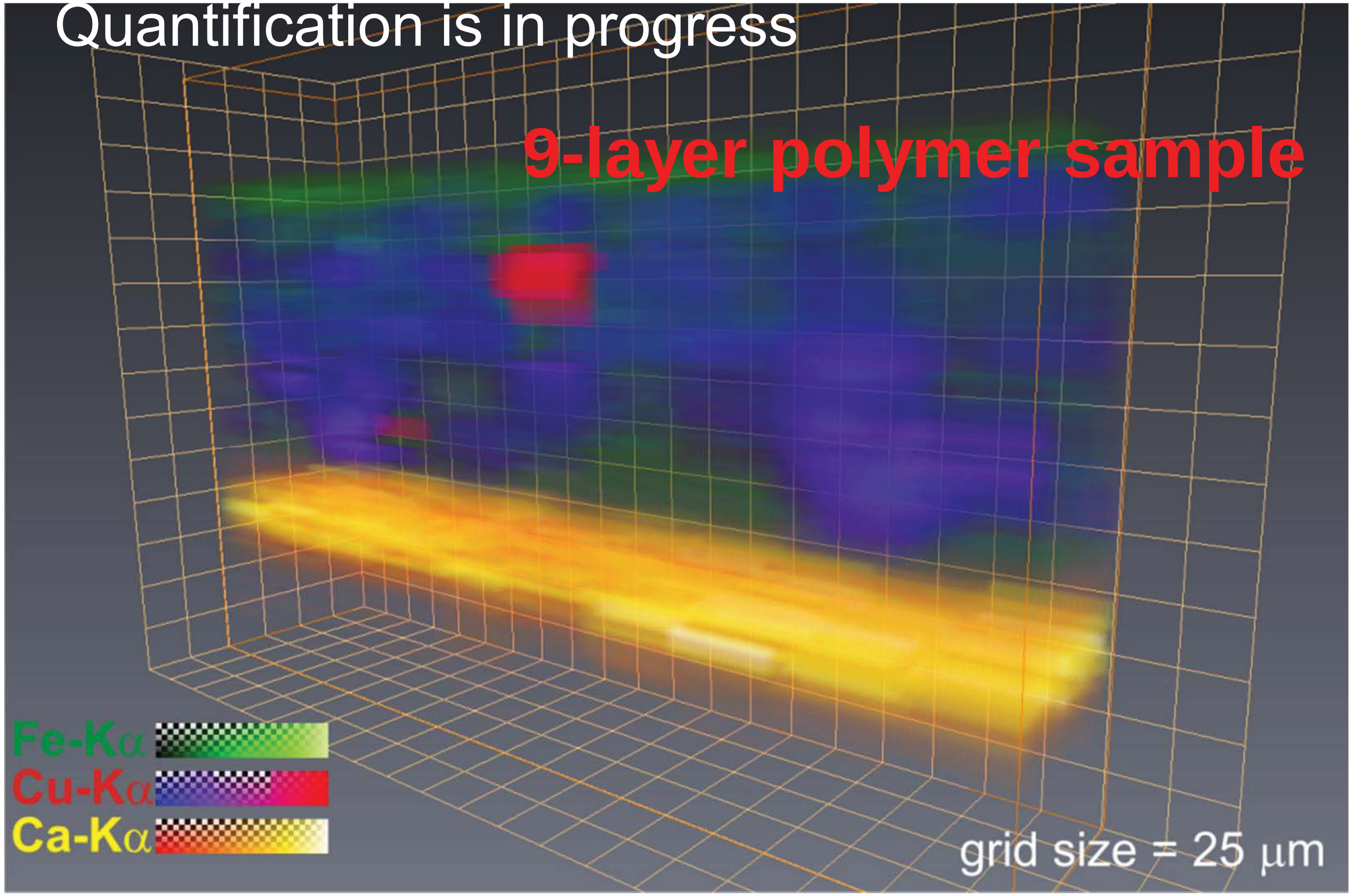

3D Micro X-Ray Absorption Fine Structure Spectroscopy

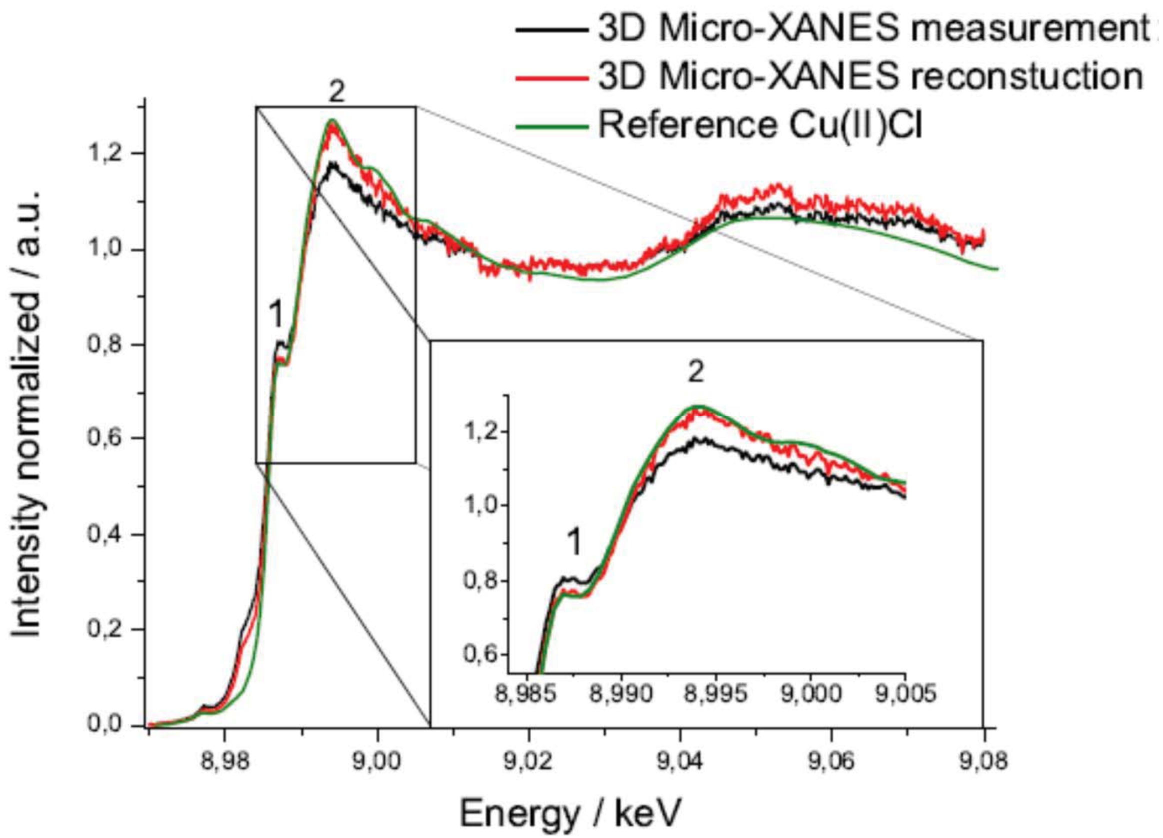

Lars Lühl et *al.*, **A reconstruction procedure for 3D Micro X-Ray Absorption Fine Structure Spectroscopy, Analytical Chemistry, DOI: 10.1021/ac202285d, (2012)**

3D Micro X-Ray Absorption Fine Structure Spectroscopy

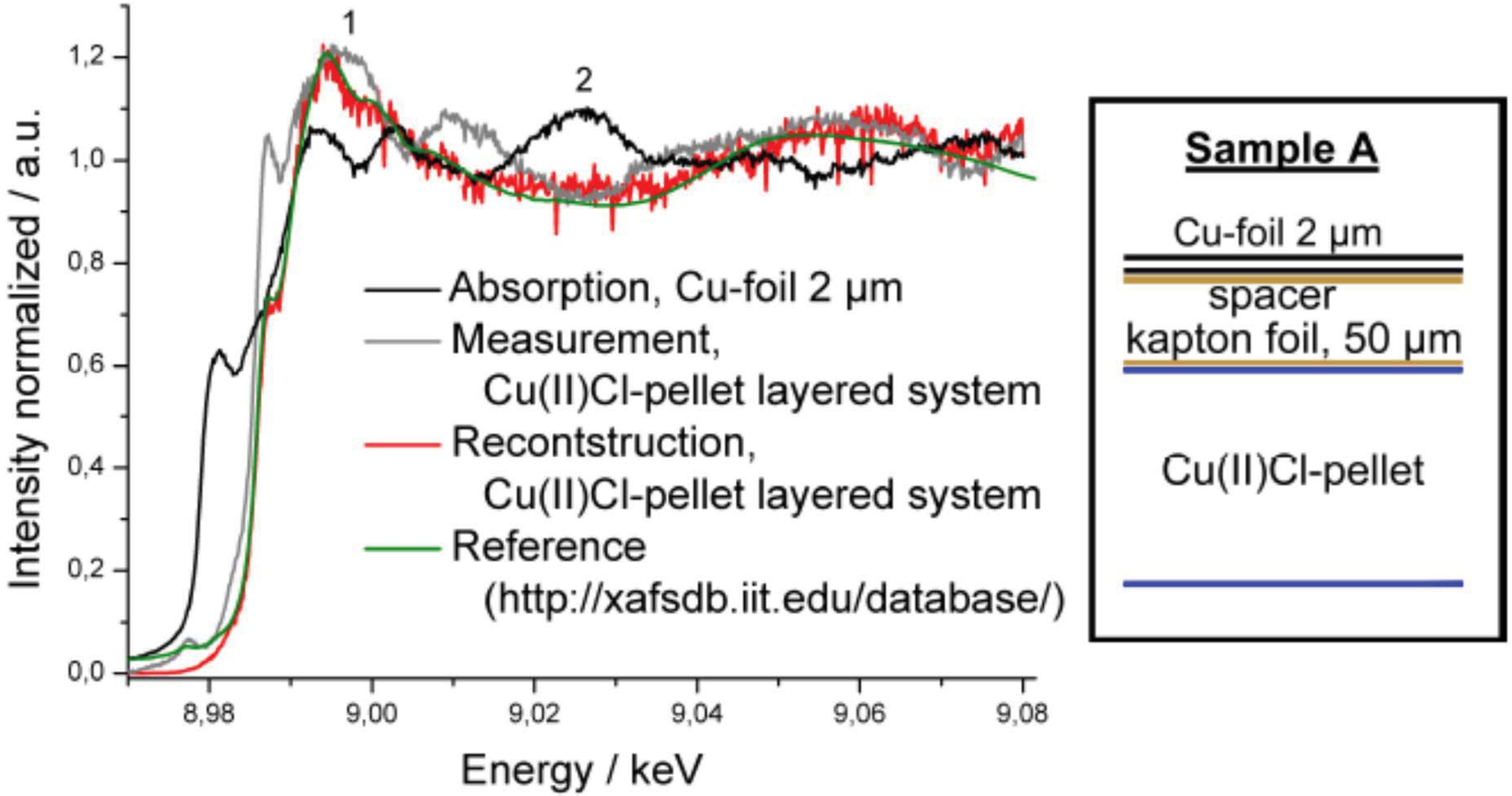

Lars Lühl et *al.*, **A reconstruction procedure for 3D Micro X-Ray Absorption Fine Structure Spectroscopy, Analytical Chemistry, DOI: 10.1021/ac202285d (2012)**

3D Chemical mapping with confocal set-up

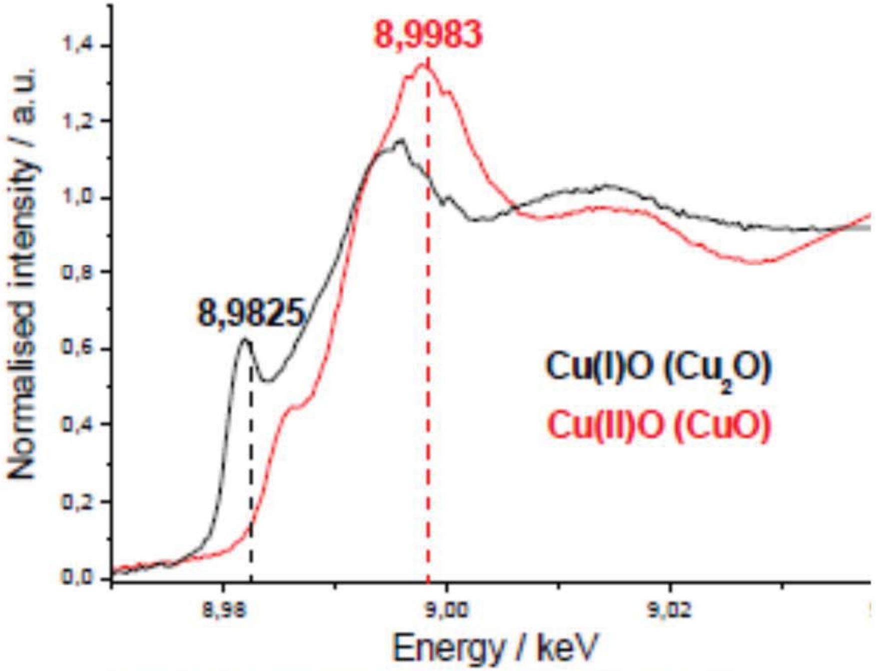

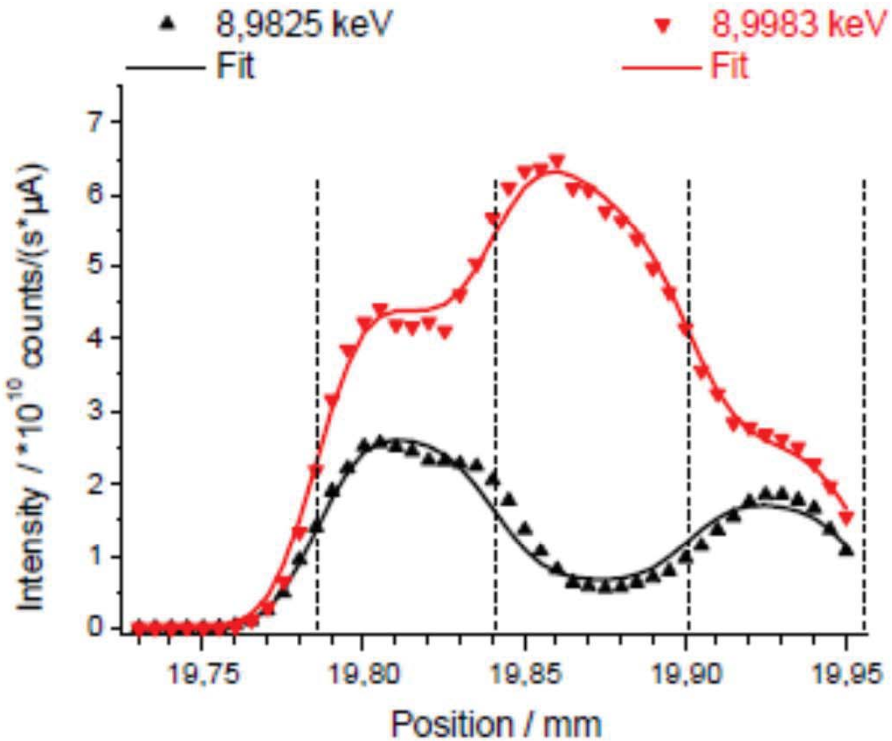

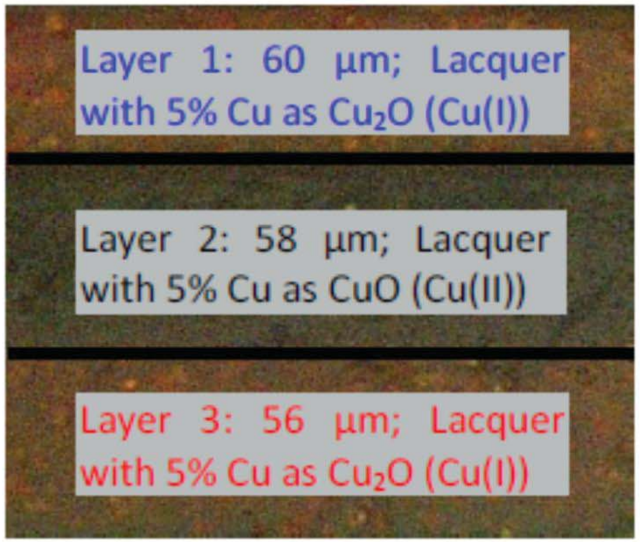

Lars Lühl et *al.*, Three-Dimensional Chemical Mapping with a Confocal XRF Setup, Anal Chem. 2013 Apr 2;85(7):3682-9.

3D Micro-XRF in Biological studies

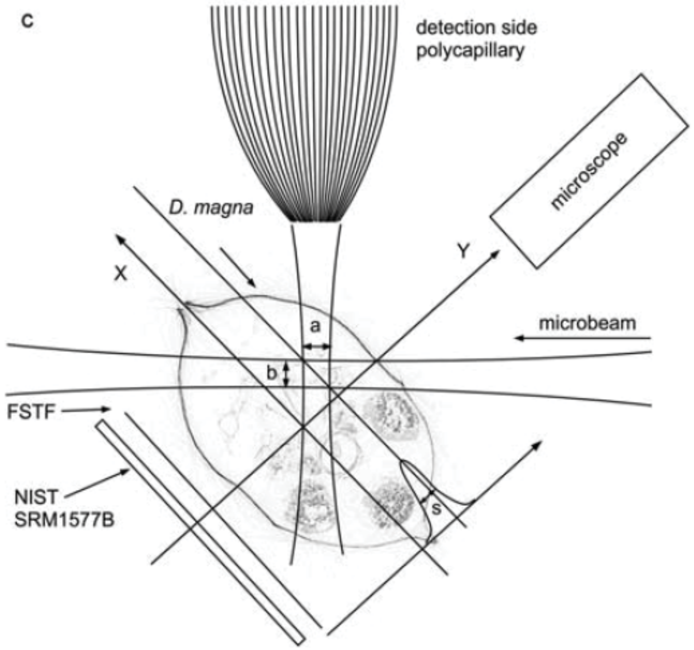

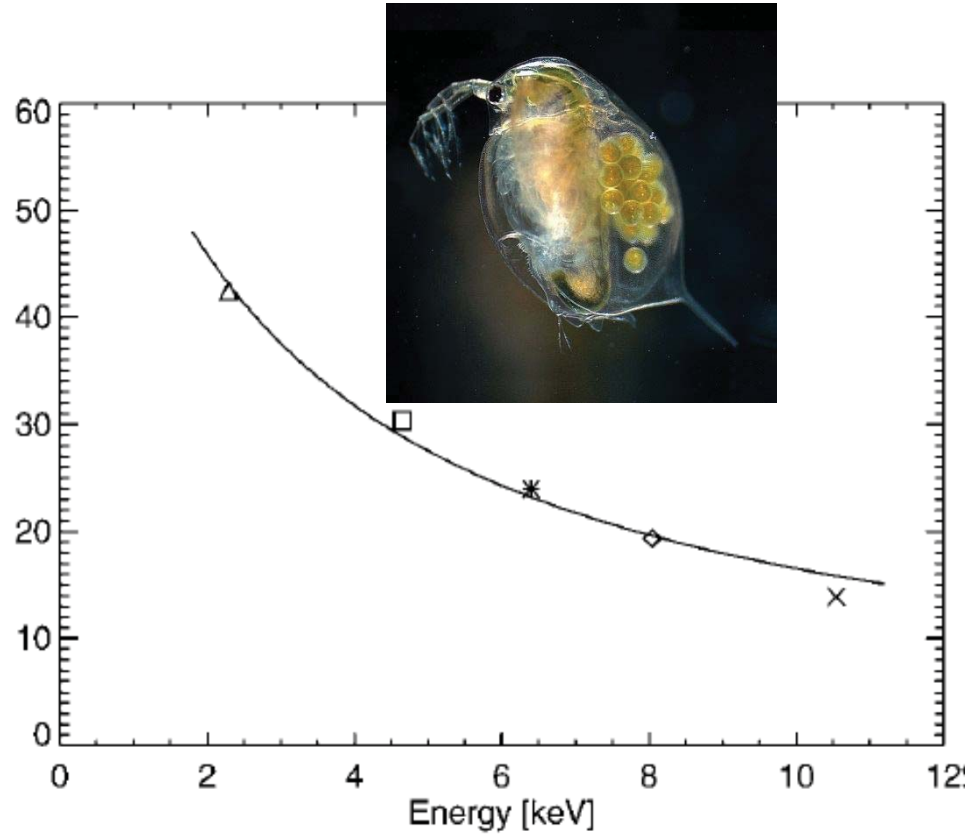

Daphnia Magna, a widely used laboratory animal for testing ecotoxicity

De Samber et *al.*, J. Anal. At. Spectrom., 2010, 25, 544–553

3D Micro-XRF in Biological studies

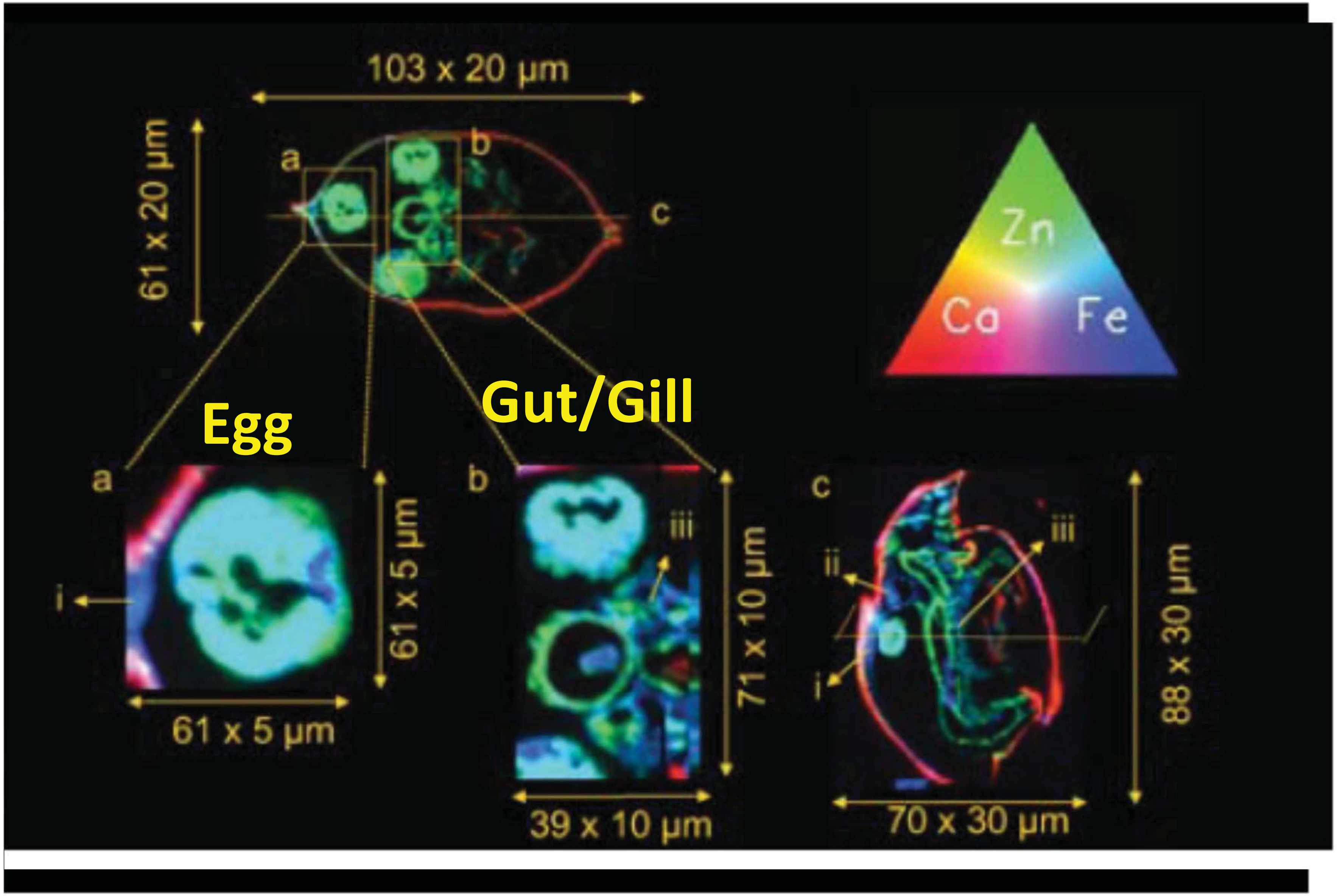

3D Micro-XRF in Biological studies

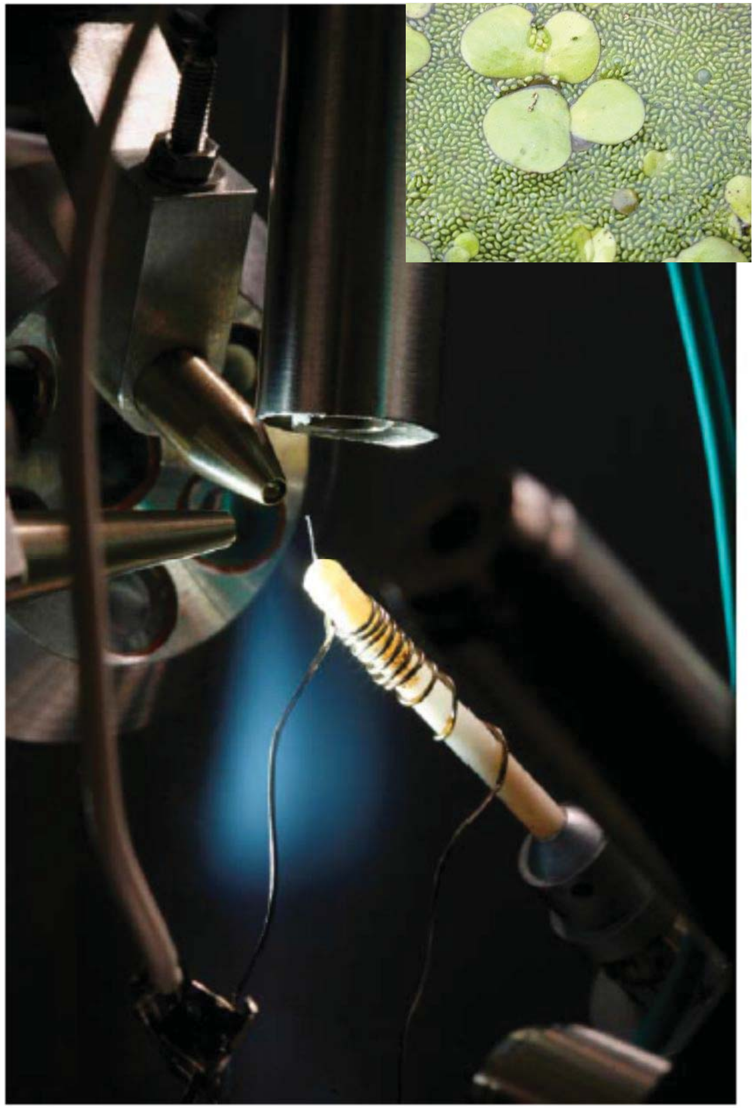

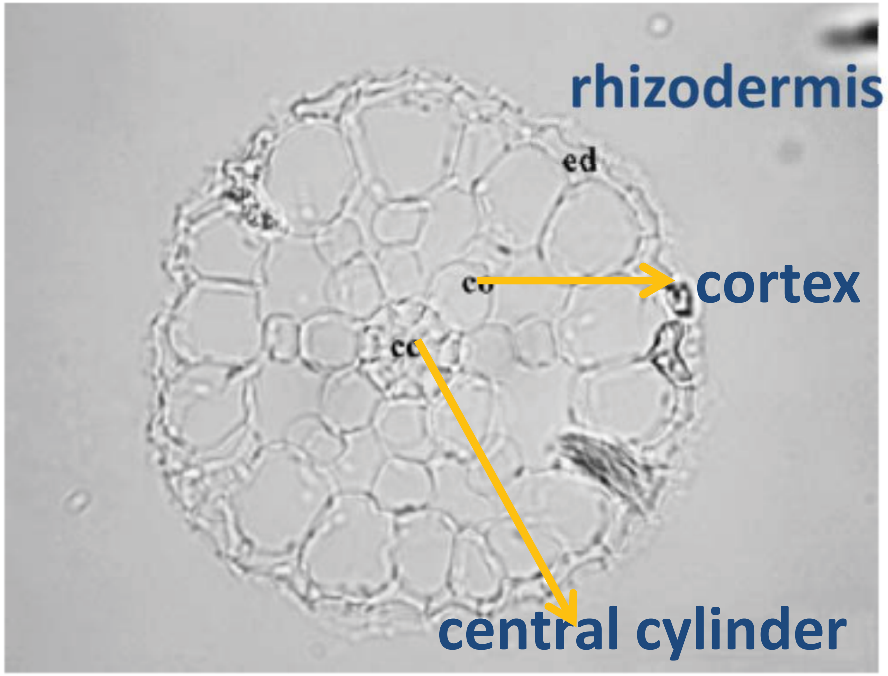

Kanngiesser et ***al***., Anal Bioanal. Chem. (2007) 389:1171–1176

Common duckweed (Lemna minor) is an important component of the aquatic food chain. The free floating plant grows on the surface of fresh water ponds and lakes

3D Micro-XRF in Biological studies

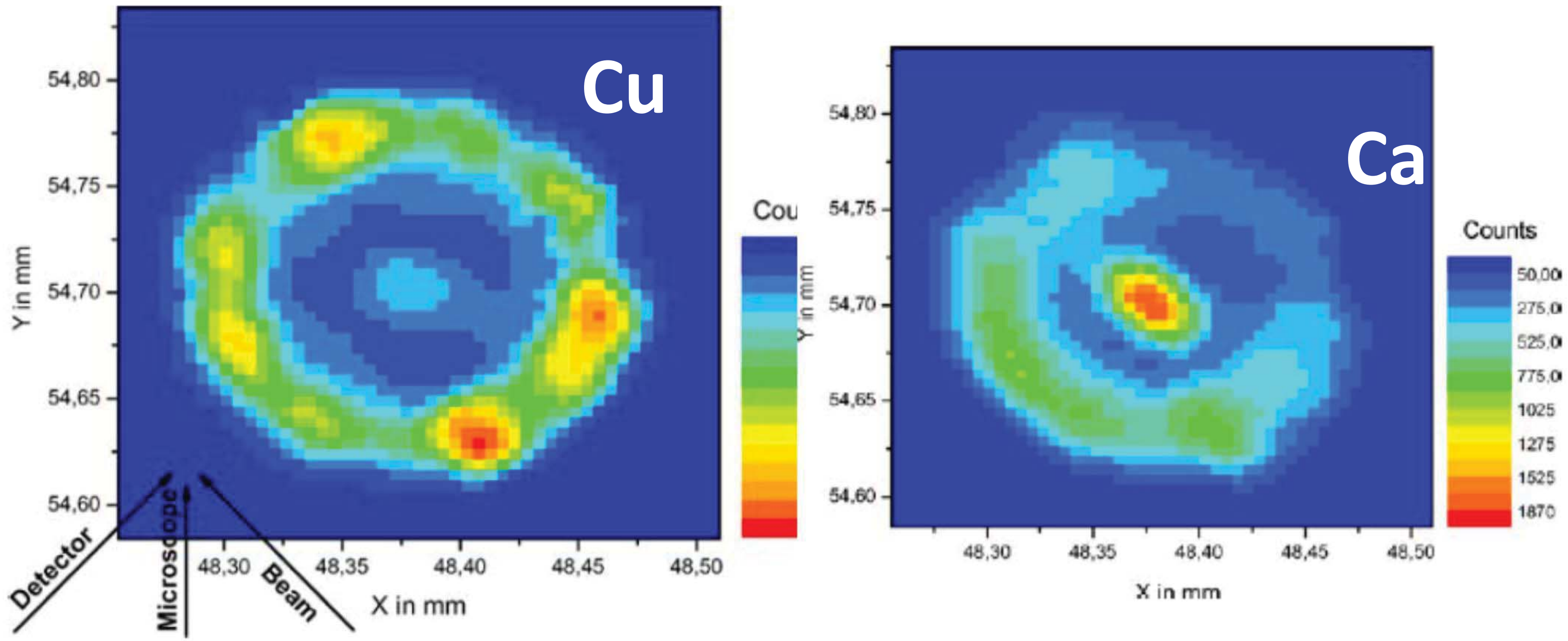

Kanngiesser et ***al***., Anal Bioanal. Chem. (2007) 389:1171–1176

3D Micro-XRF in Medicine

Backscattered Electron (BE) image of the analyzed 200 µm thick patella sample

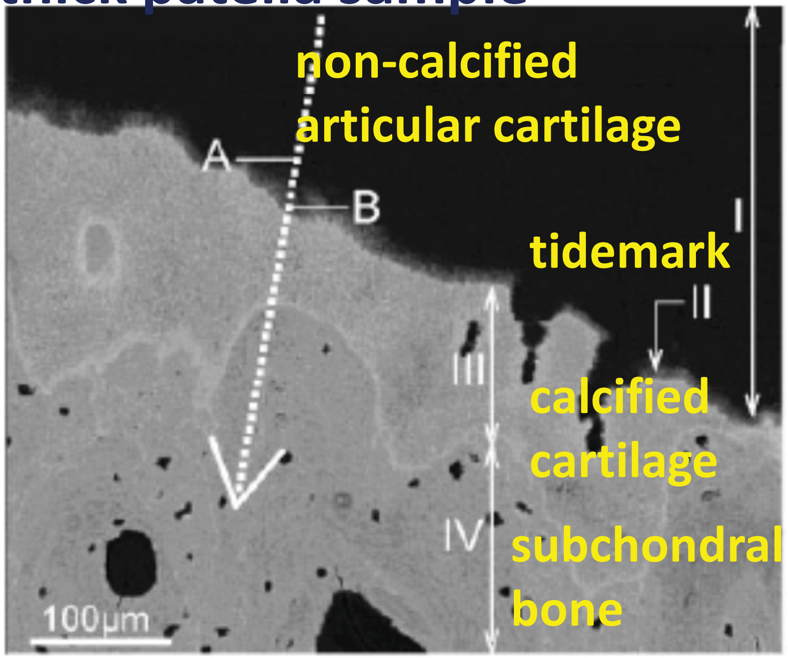

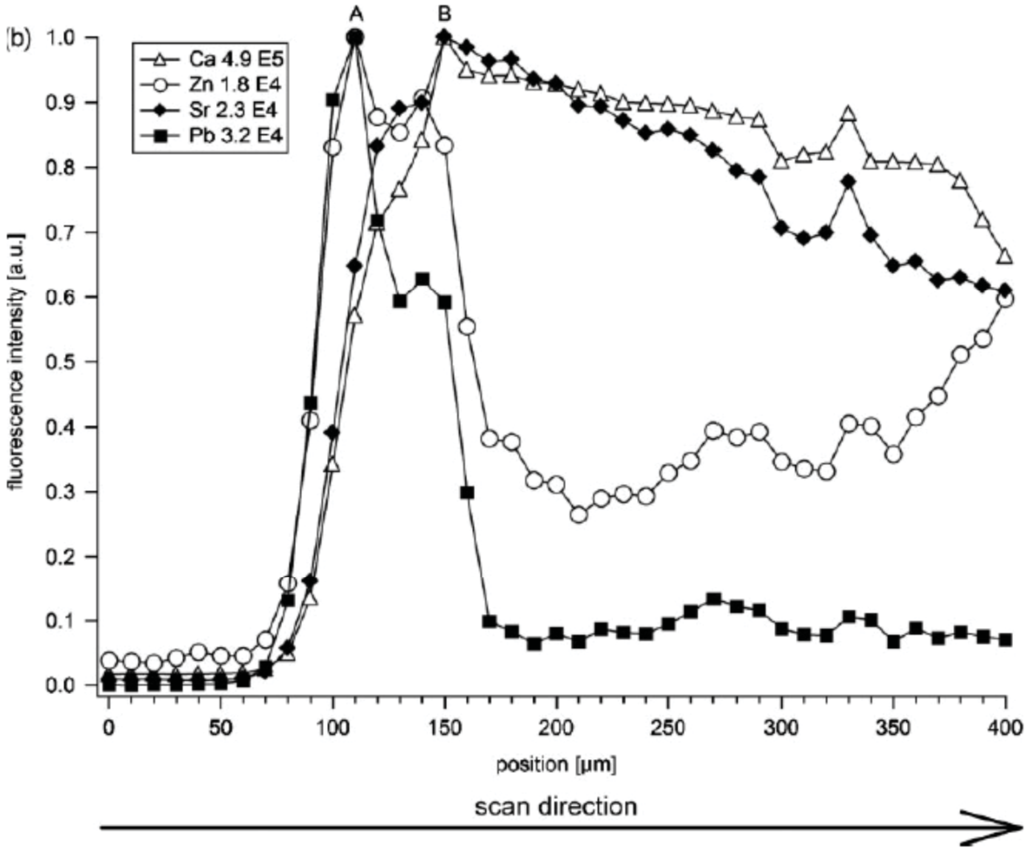

Zoeger et al, Determination of the elemental distribution in human joint bones by SR micro XRF, *X-Ray Spectrom.* 2008; 37: 3–11

3D Micro-XRF in Medicine

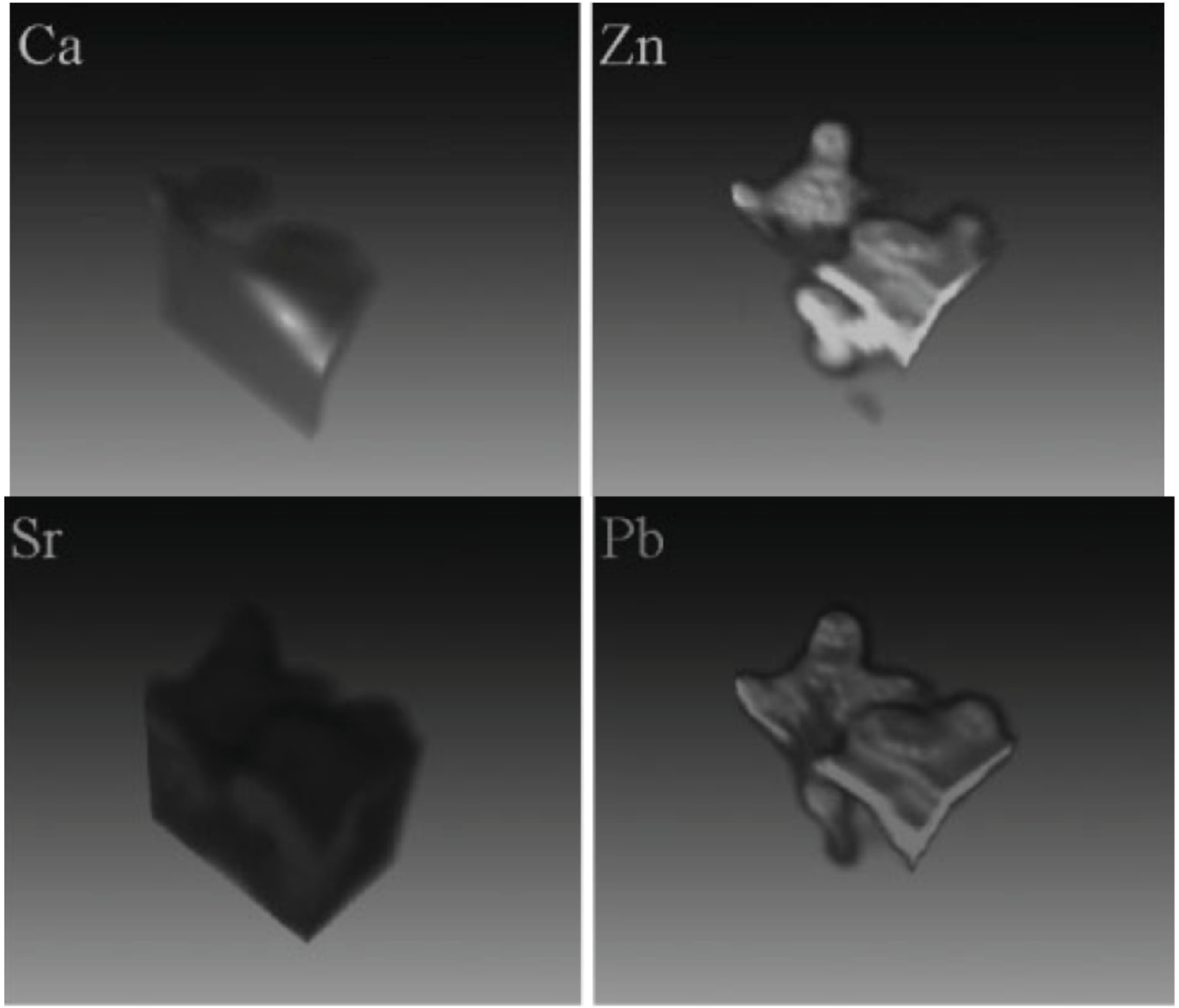

3D Micro-XRF in planetary science

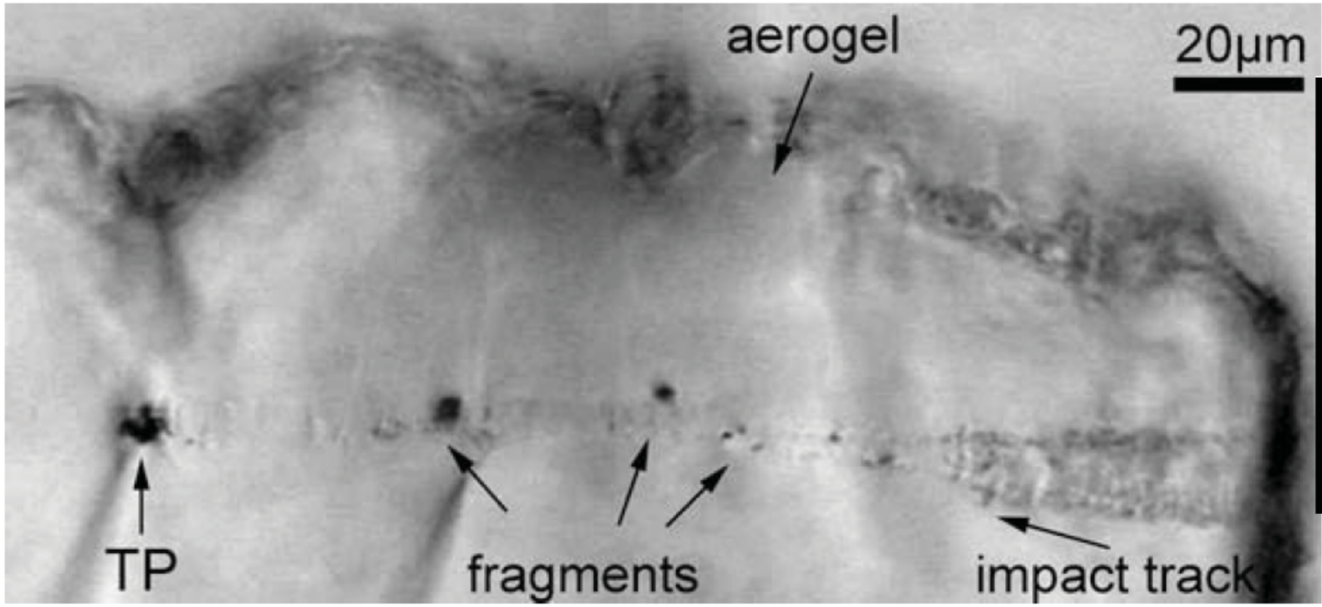

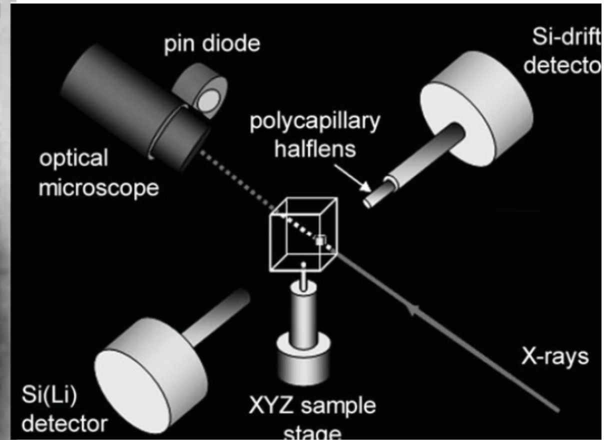

S. Schmitz et *al.*, In situ identification of a CAI candidate in 81P/Wild 2 cometary, dust by confocal high resolution synchrotron X-ray fluorescence
Geochimica et Cosmochimica Acta 73 (2009) 5483–5492

3D Micro-XRF in planetary science

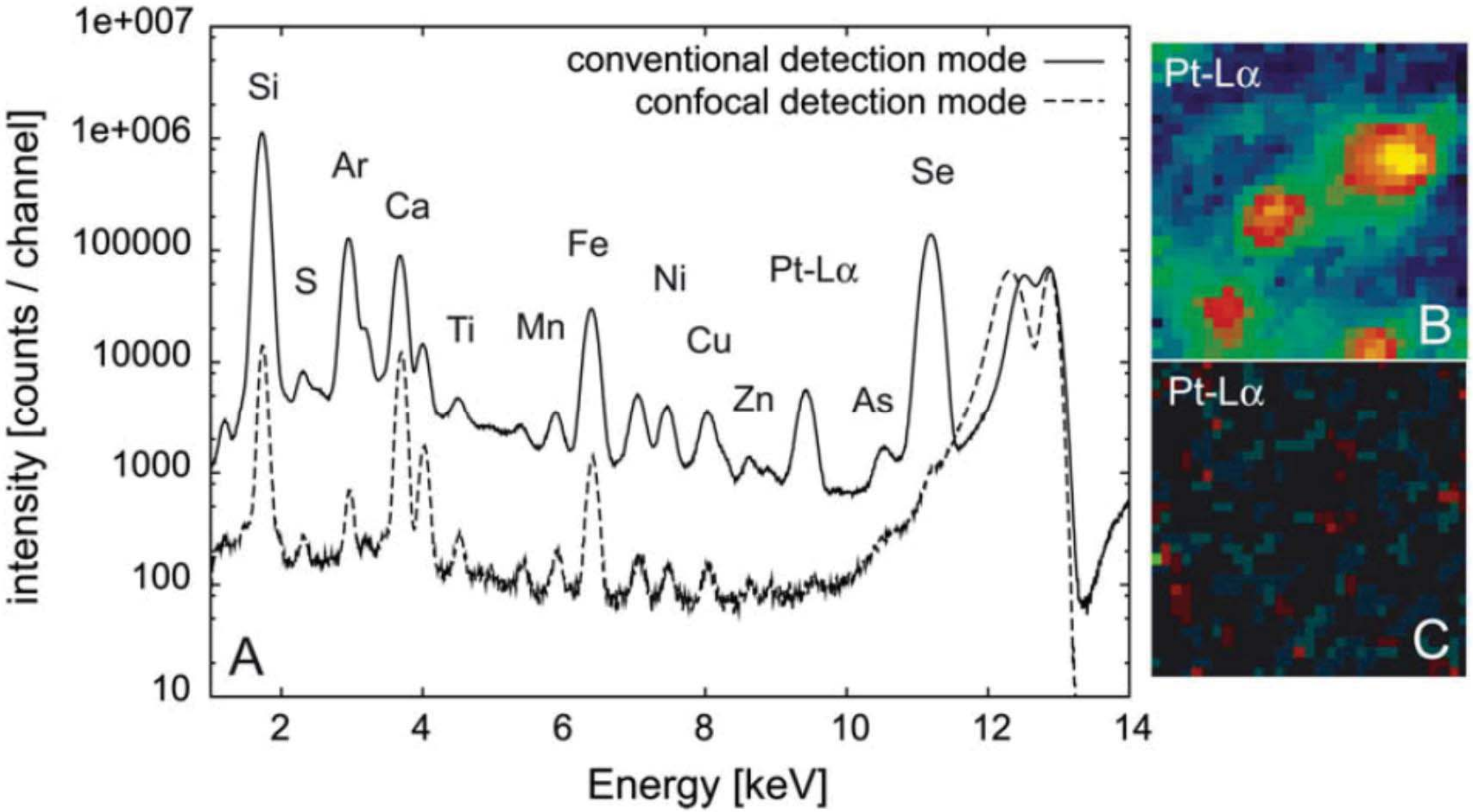

300 nm x 300 nm
9×10^7 ph/s
19 um/Fe-Kα

3D Micro-XRF in planetary science

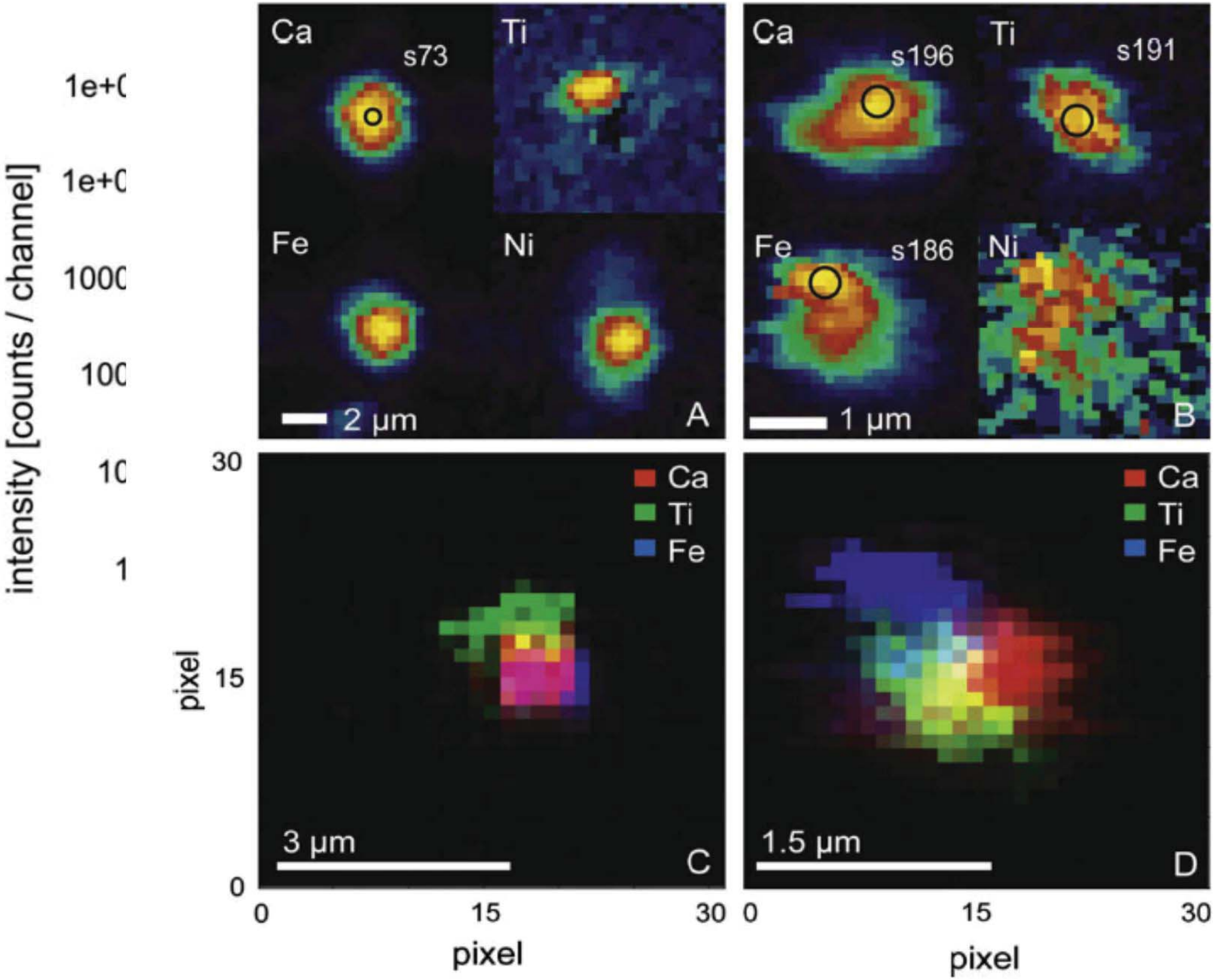

300 nm x
300 nm
$9x10^7$ ph/s
19 um/Fe-Kα

Plant nutrition-transport: Uptake of Fe by tomato roots

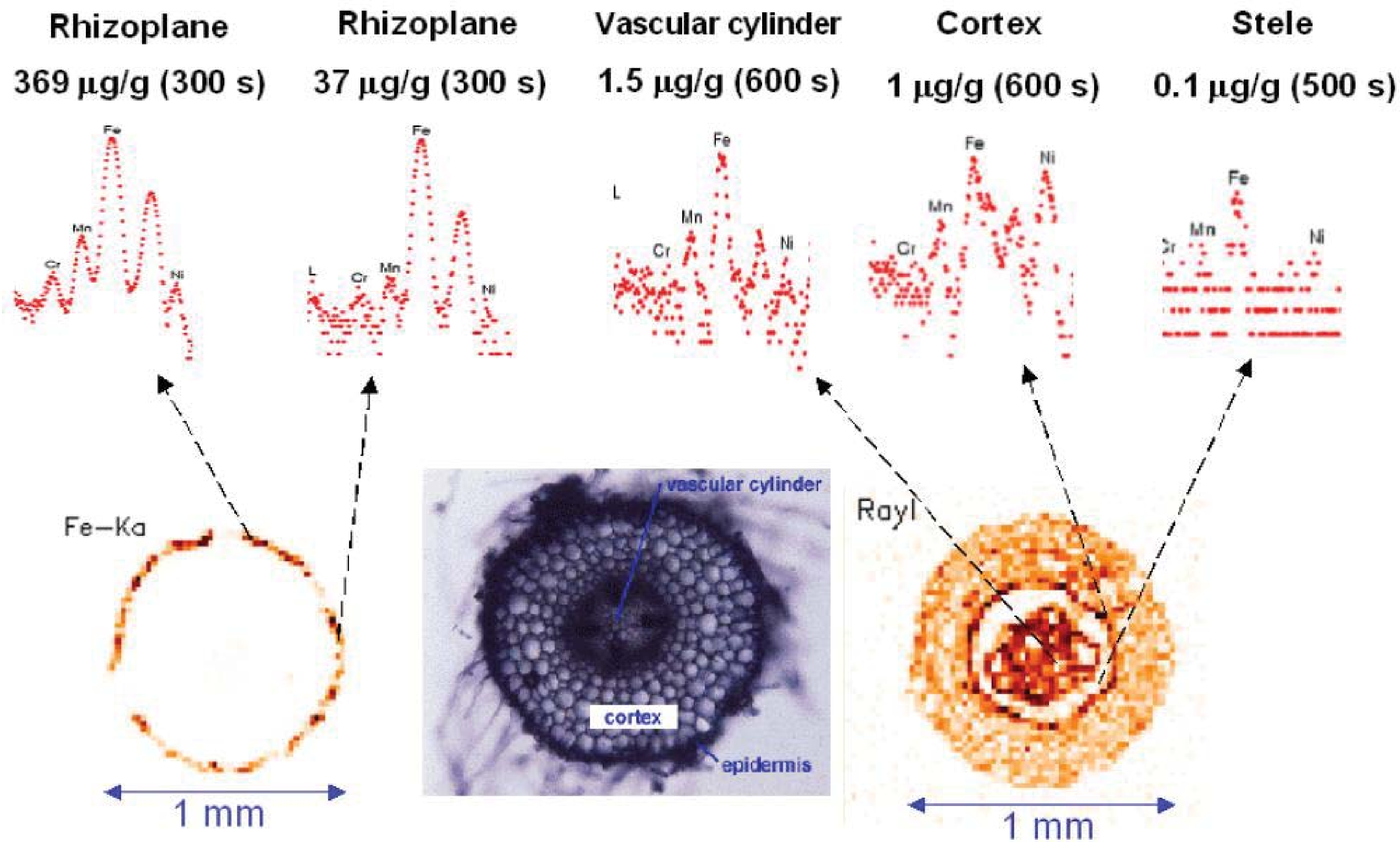

Plant nutrition/transport: Uptake of heavy metals

A. Straczek, et *al.*, J. of Environmental Radioactivity 101(3), 258-266 (2010).

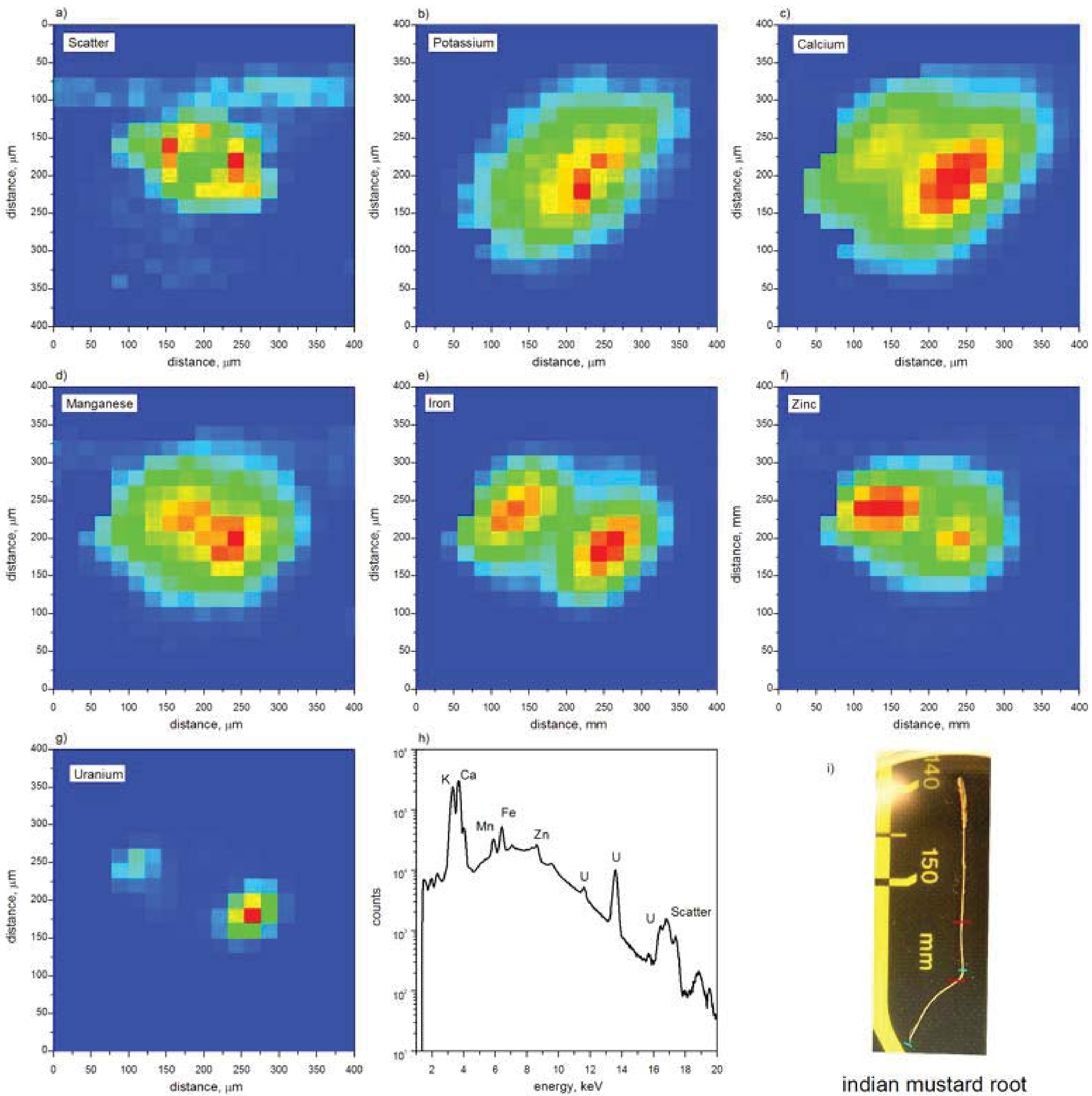

Plant nutrition-transport: Uptake of heavy metals – Uranium

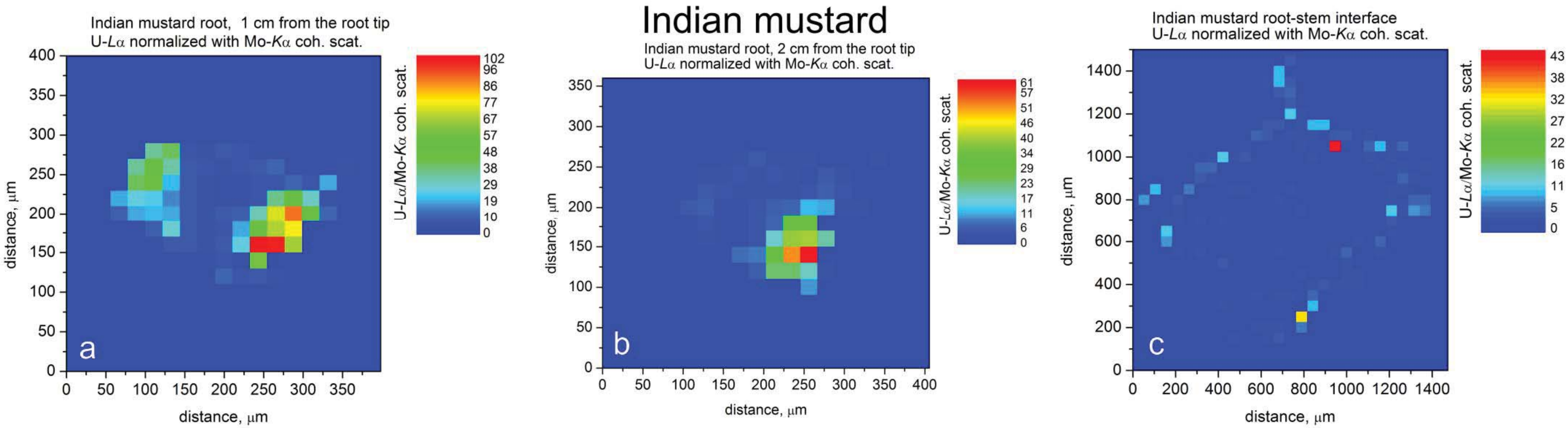

A. Straczek, et *al.*, J. of Environmental Radioactivity 101(3), 258-266 (2010).

3D Micro-XRF applications in Geology

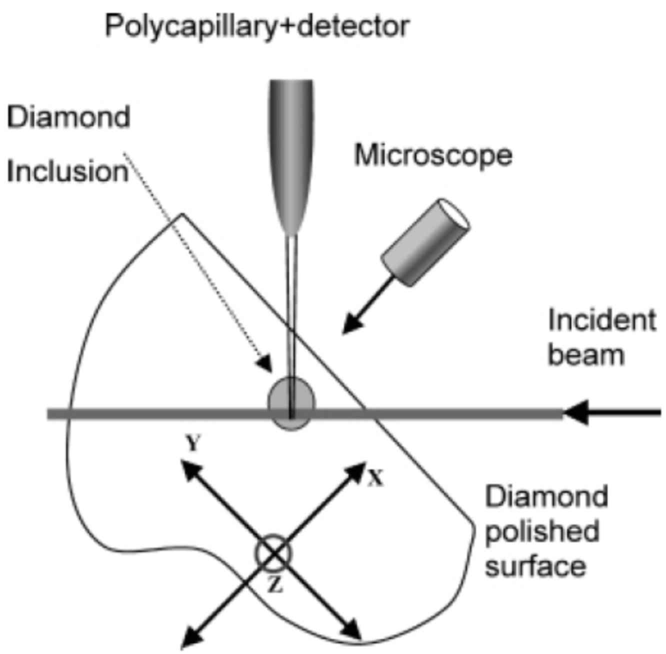

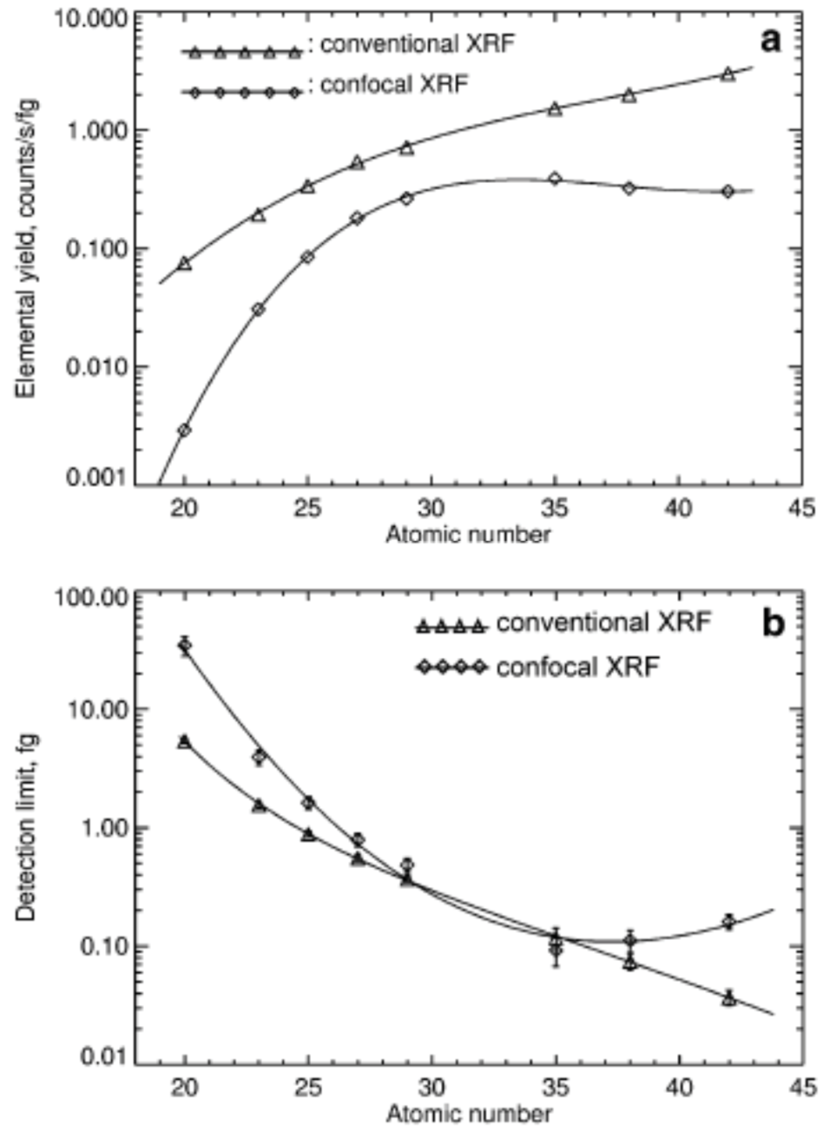

Vincze et *al*, Anal. Chem. 2004, 76, 6786-6791

28 keV, 2 um (V) X 5 um (H), 10^{10} photons/s.

3D Micro-XRF applications in Geology

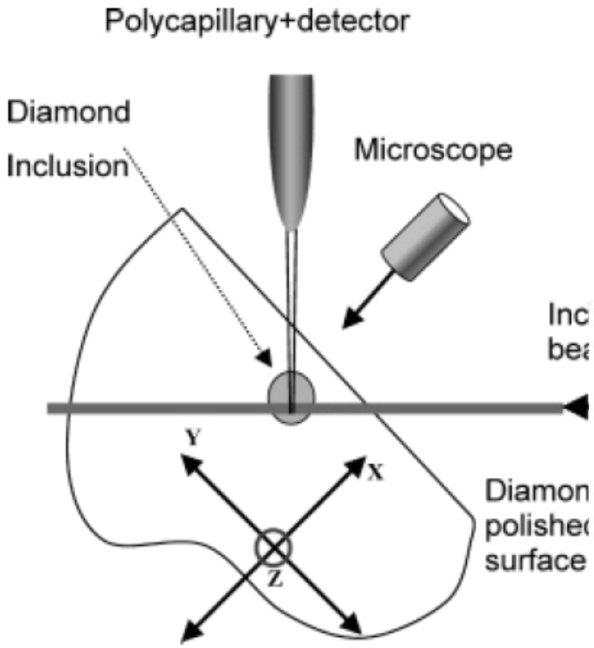

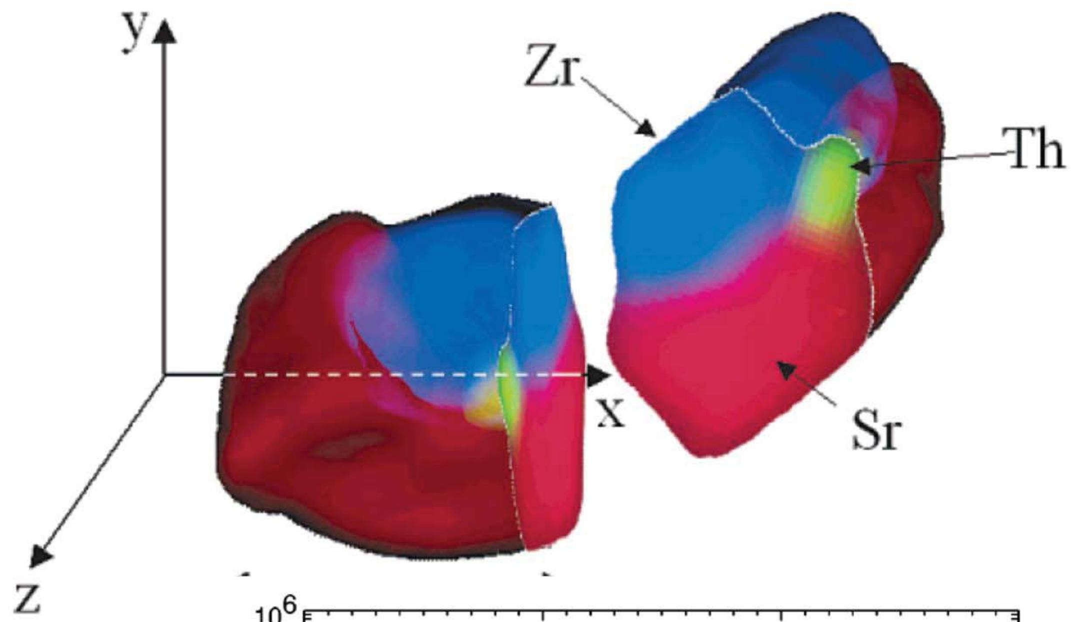

Vincze et *al*, Anal. Chem. 2004, 76, 6786-6791

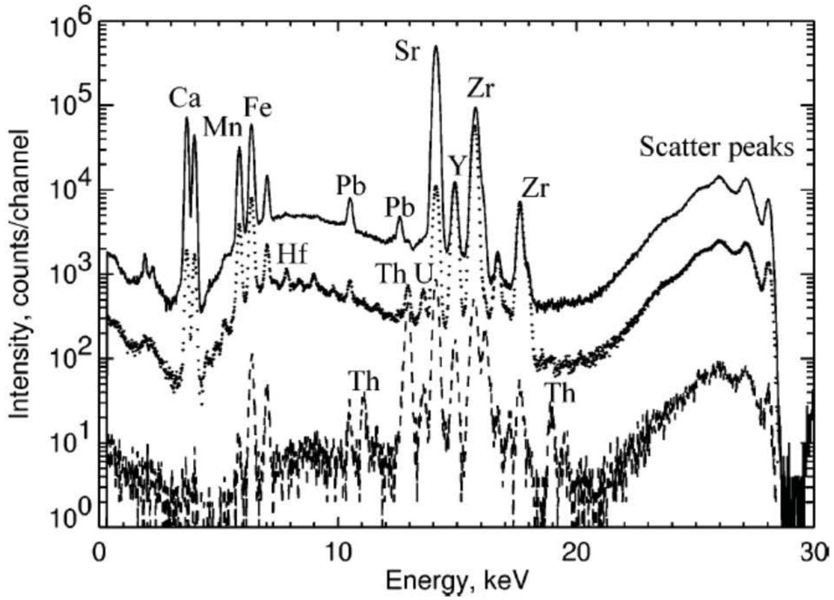

28 keV, 2 um (V) X 5 um (H), 10^{10} photons/s.

3D analysis of Roman period (2 cent BC) painted plasters @IAEA Laboratories

In support of understanding the elaboration of raw materials and application of painting techniques in antiquity.

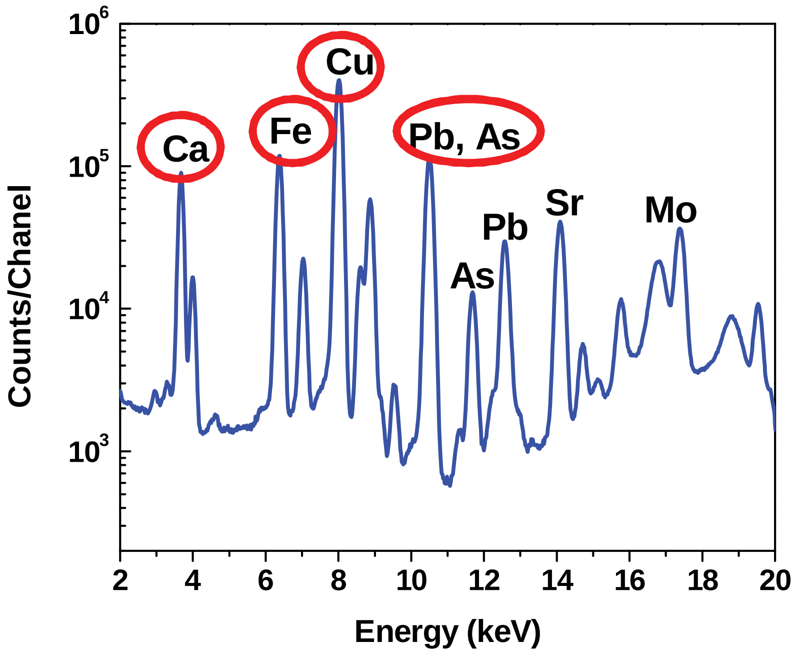

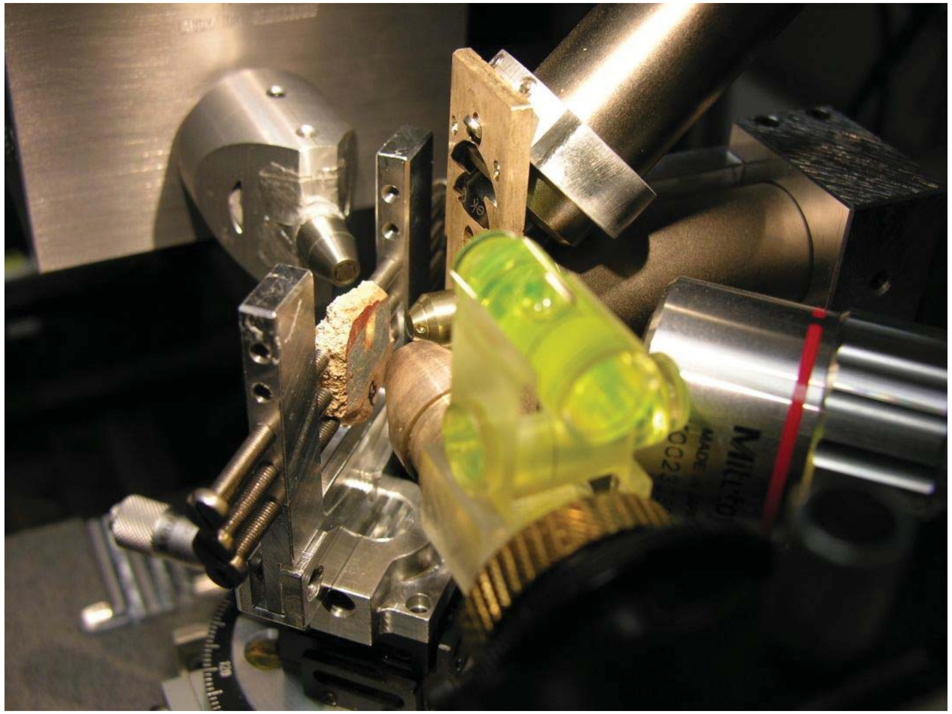

Micro-XRF spectrum from the analysis on extended area

3D analysis of Roman period (2 cent BC) painted plasters @IAEA Laboratories

Egyptian Blue (Cu)
Red ochre (Fe)

Pb and As are constituents trace-minor elements of the iron based ochre paint layer

Volume:
20 µm x 1440 µm x 293 µm,
xyz scanning spacing:
40 µm X 40 µm x 3 µm

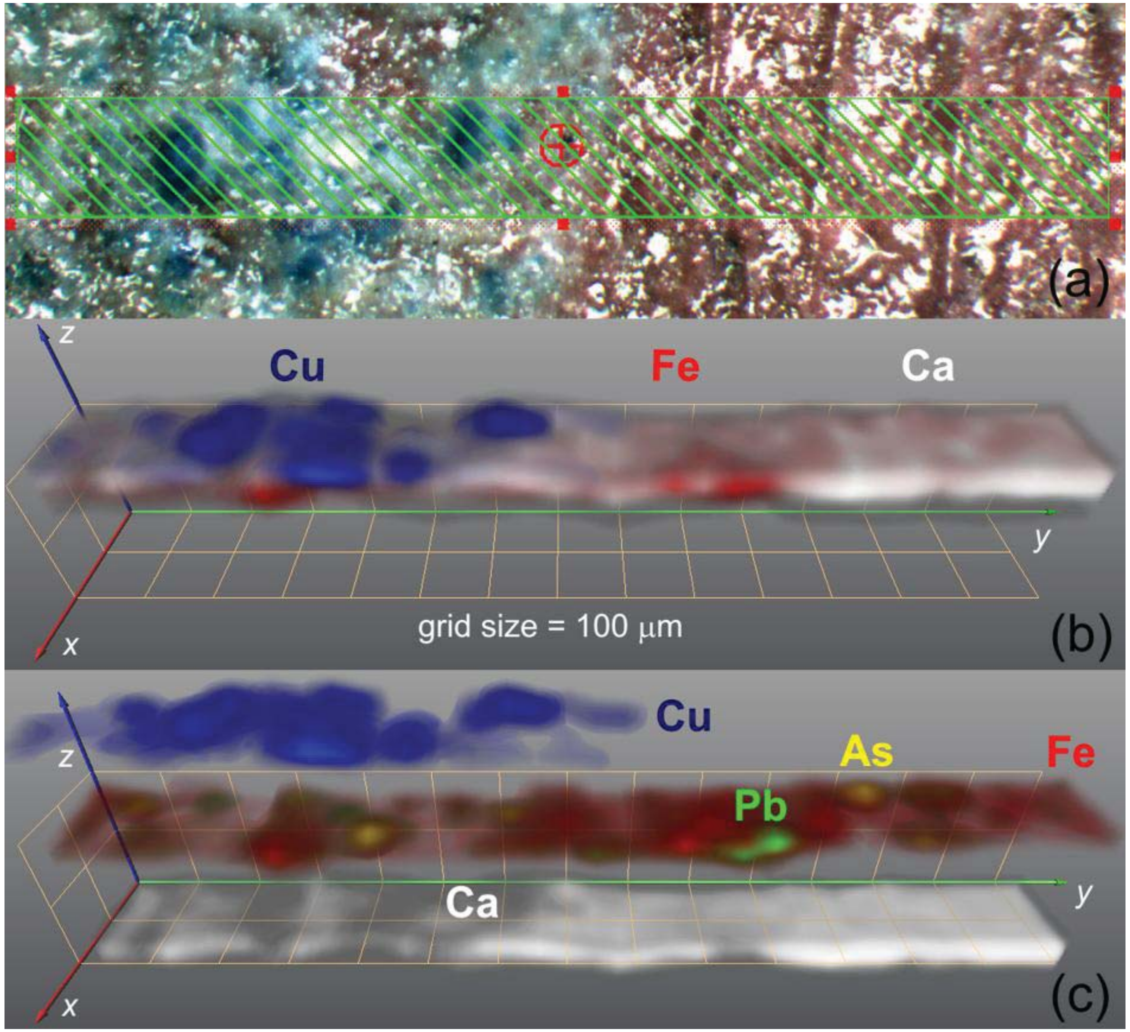

3D analysis of Roman period (2nd cent. BC) painted plasters @IAEA Laboratories

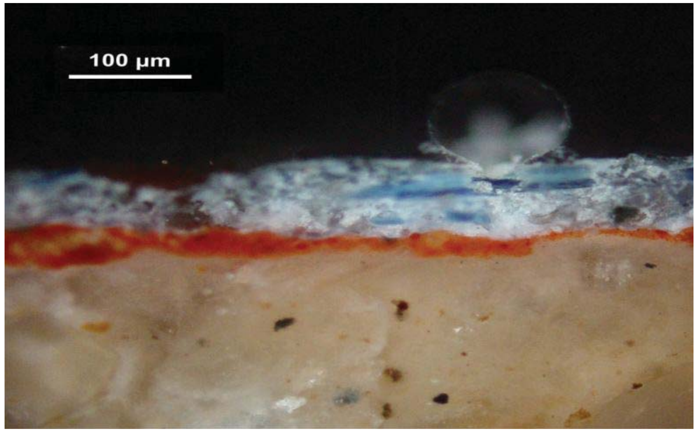

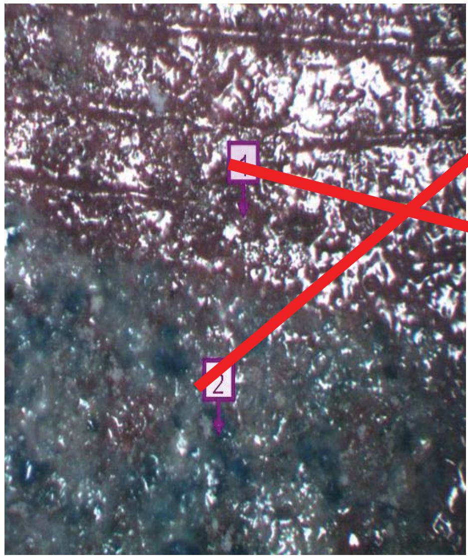

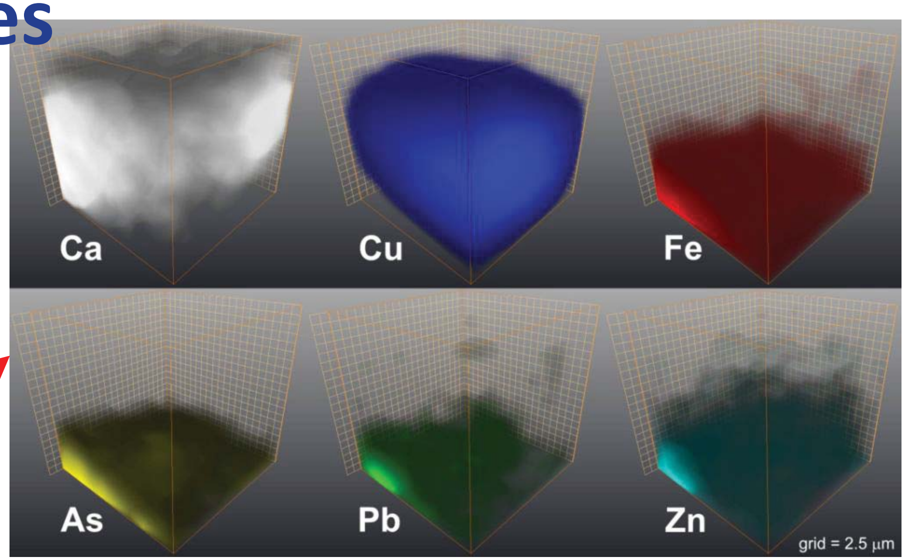

56 µm/55 µm/55µm
5.6 µm/5.5 µm/5µm

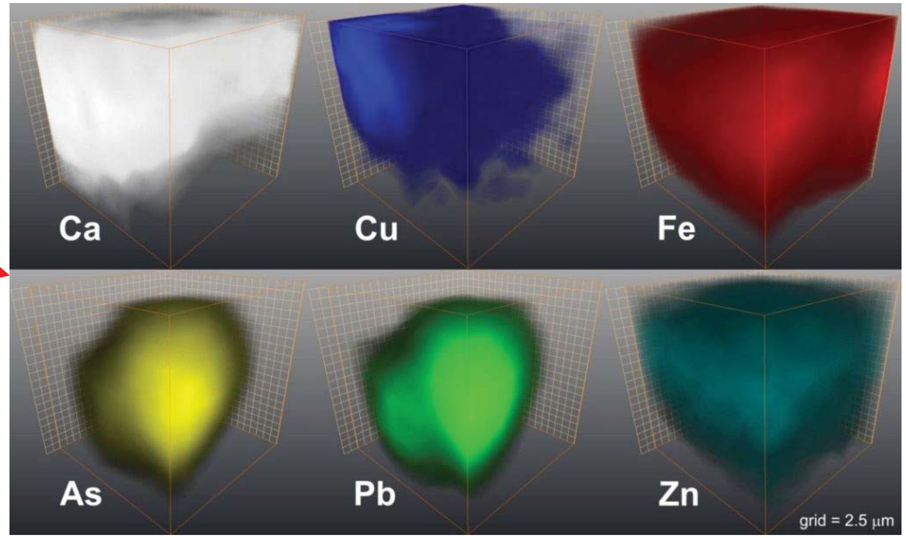

Identification of minor micro-components

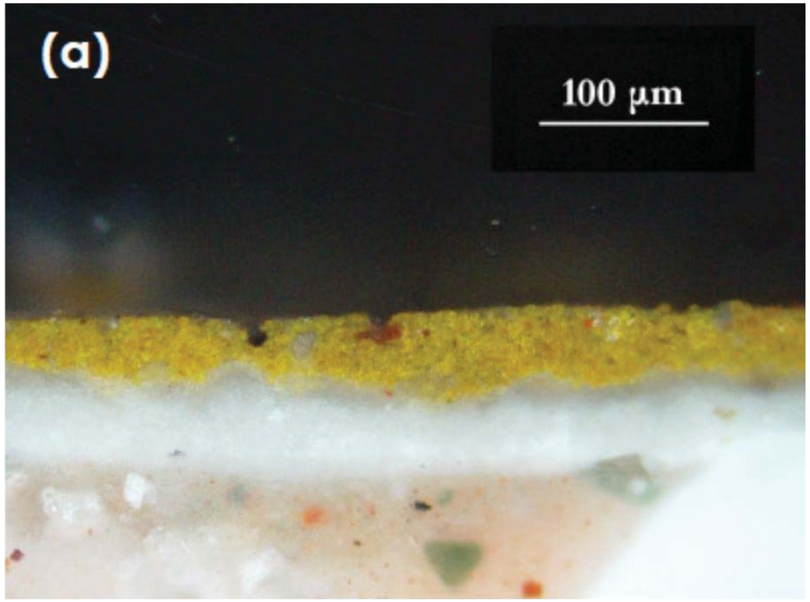

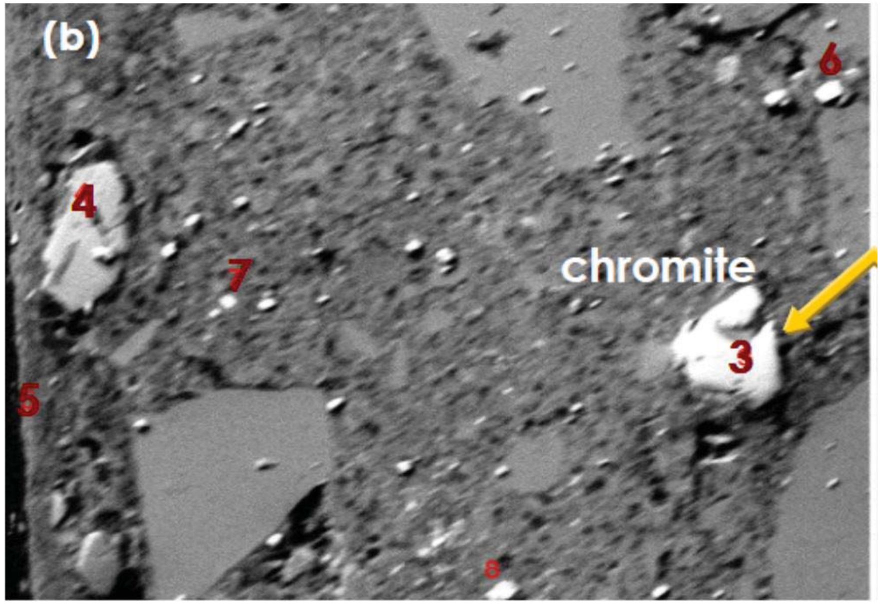

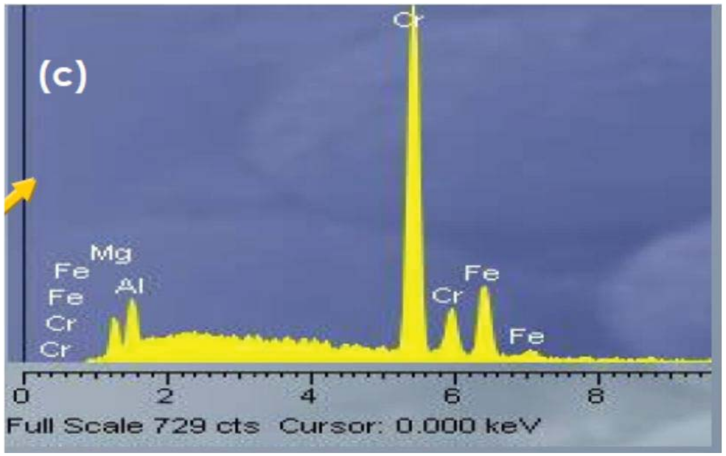

Chromite: $(Mg, Fe^{2+})(Cr, Al)_2O_4)$

Collaboration with Technical University of Crete and National Research Foundation – KERAS

Samples: courtesy by H. Brecoulaki, KERAS

Identification of minor micro-components

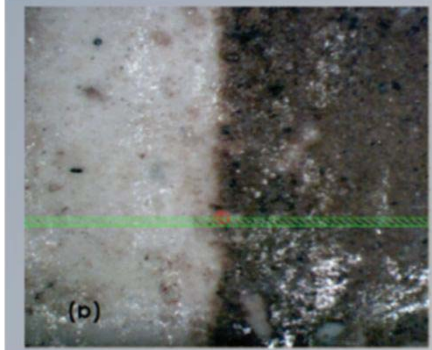

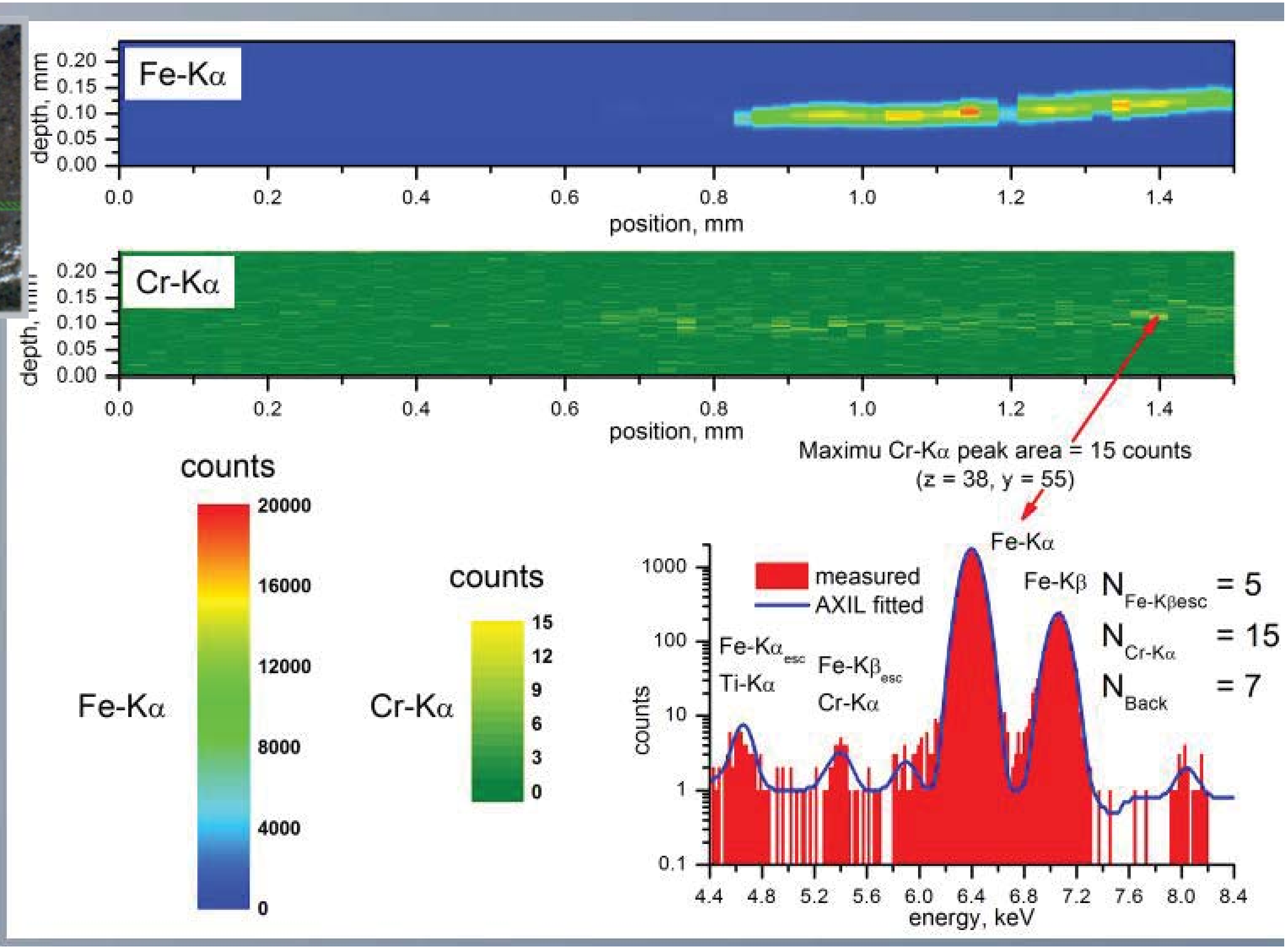

Elemental depth profiling of Japanese lacquerware ‘Tamamushi-nuri’

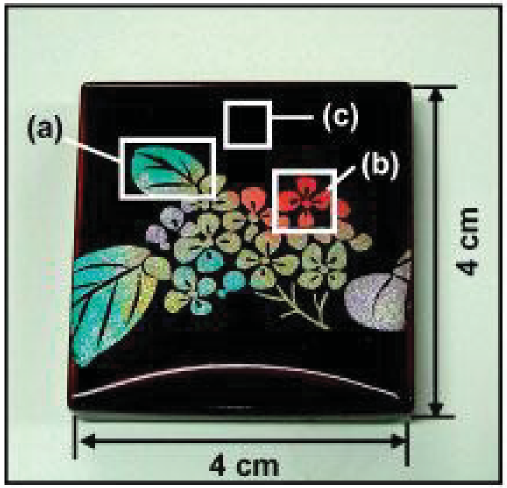

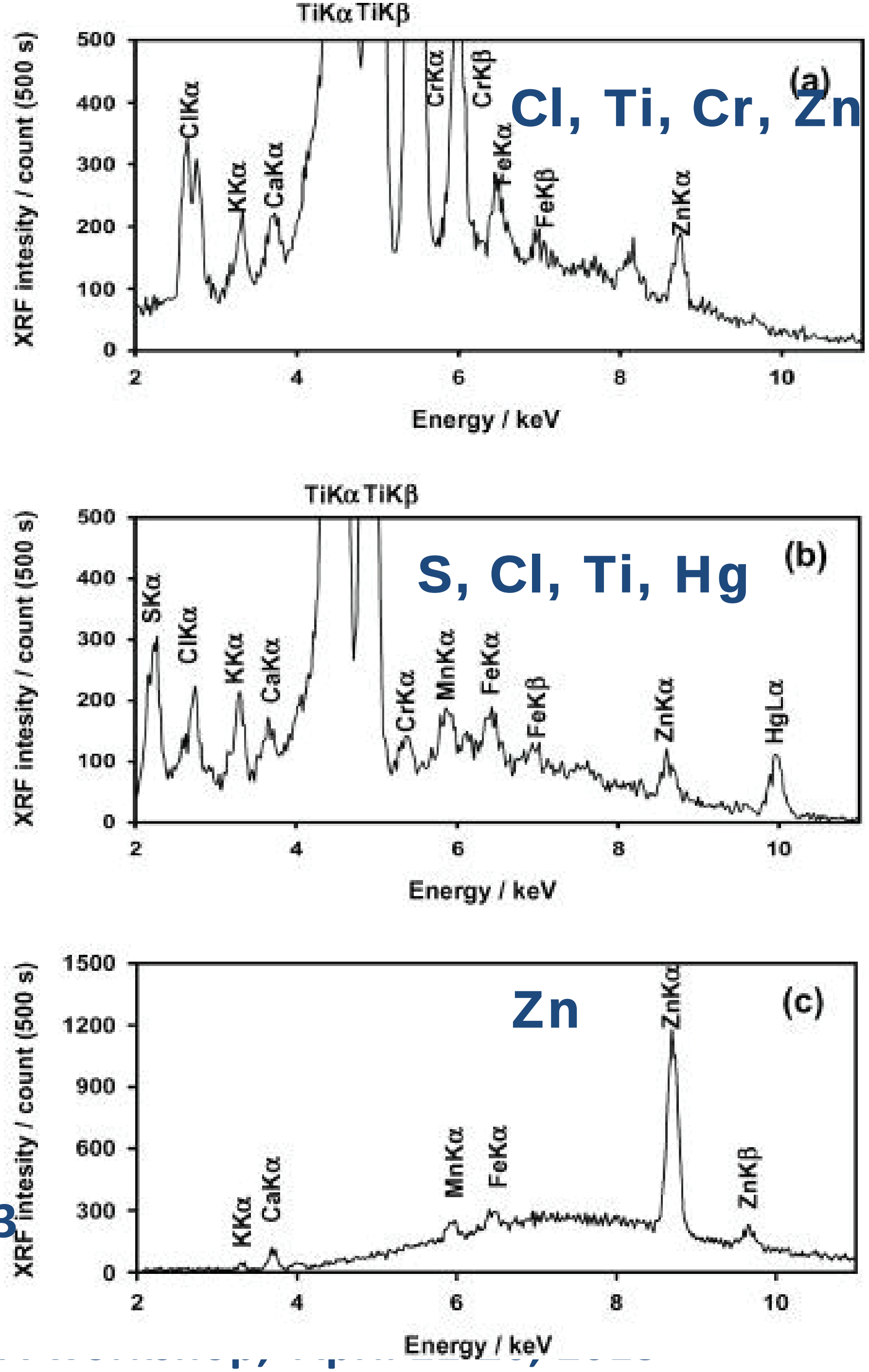

Titan white (TiO_2) as a white pigment. Cr K lines indicate the presence of green pigment, i.e. chromium oxide (Cr_2O_3) or viridian ($Cr_2O(OH)_4$). Hg L and S K lines suggest the red pigment of cinnabar (HgS)

Nakano, Tsuji, XRS 2008, DOI 10.1002/xrs.1163

Elemental depth profiling of Japanese lacquerware 'Tamamushi-nuri'

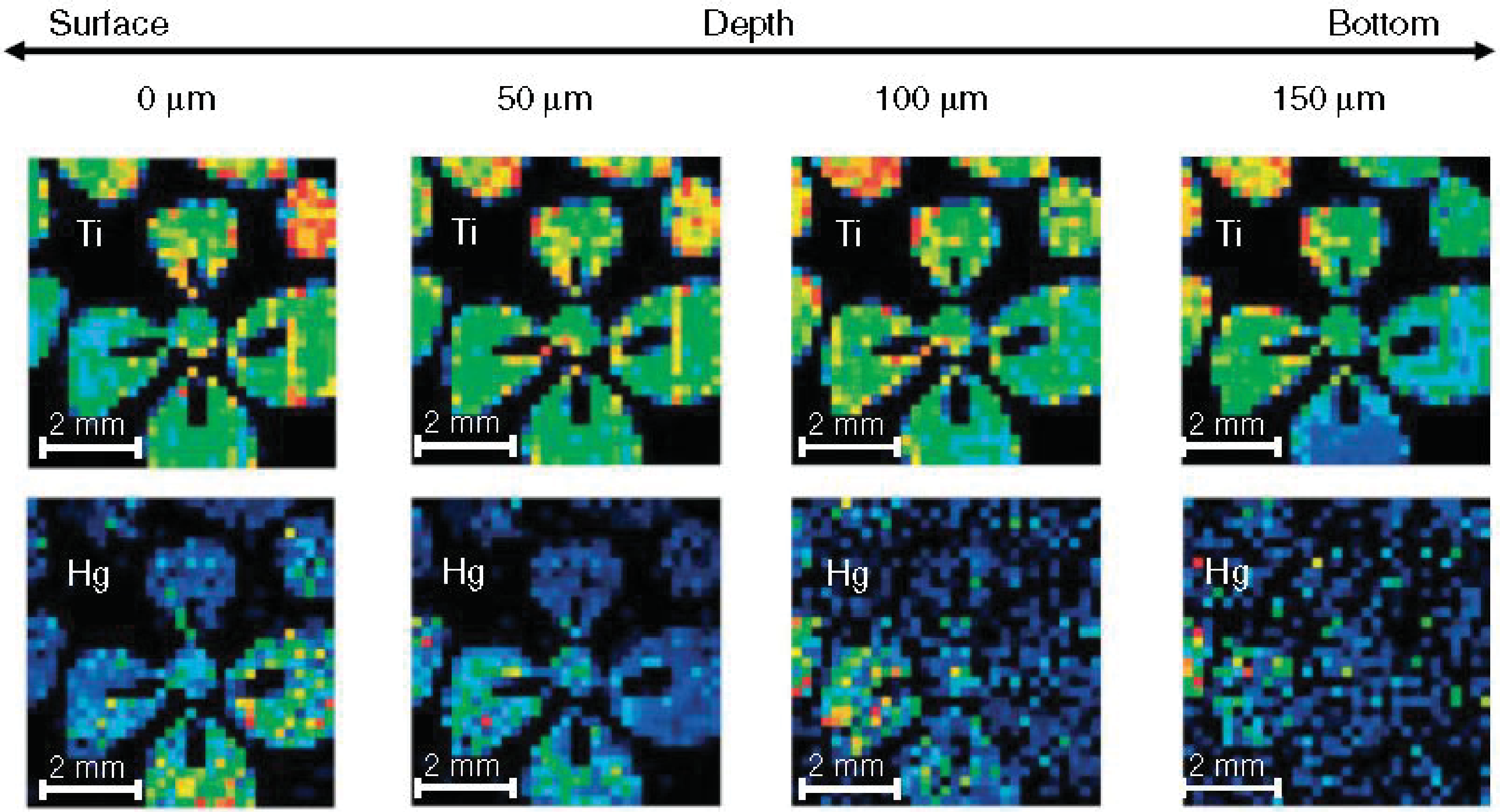

Nakano, Tsuji, XRS 2008, DOI 10.1002/xrs.1163

Elemental depth profiling of Japanese lacquerware 'Tamamushi-nuri'

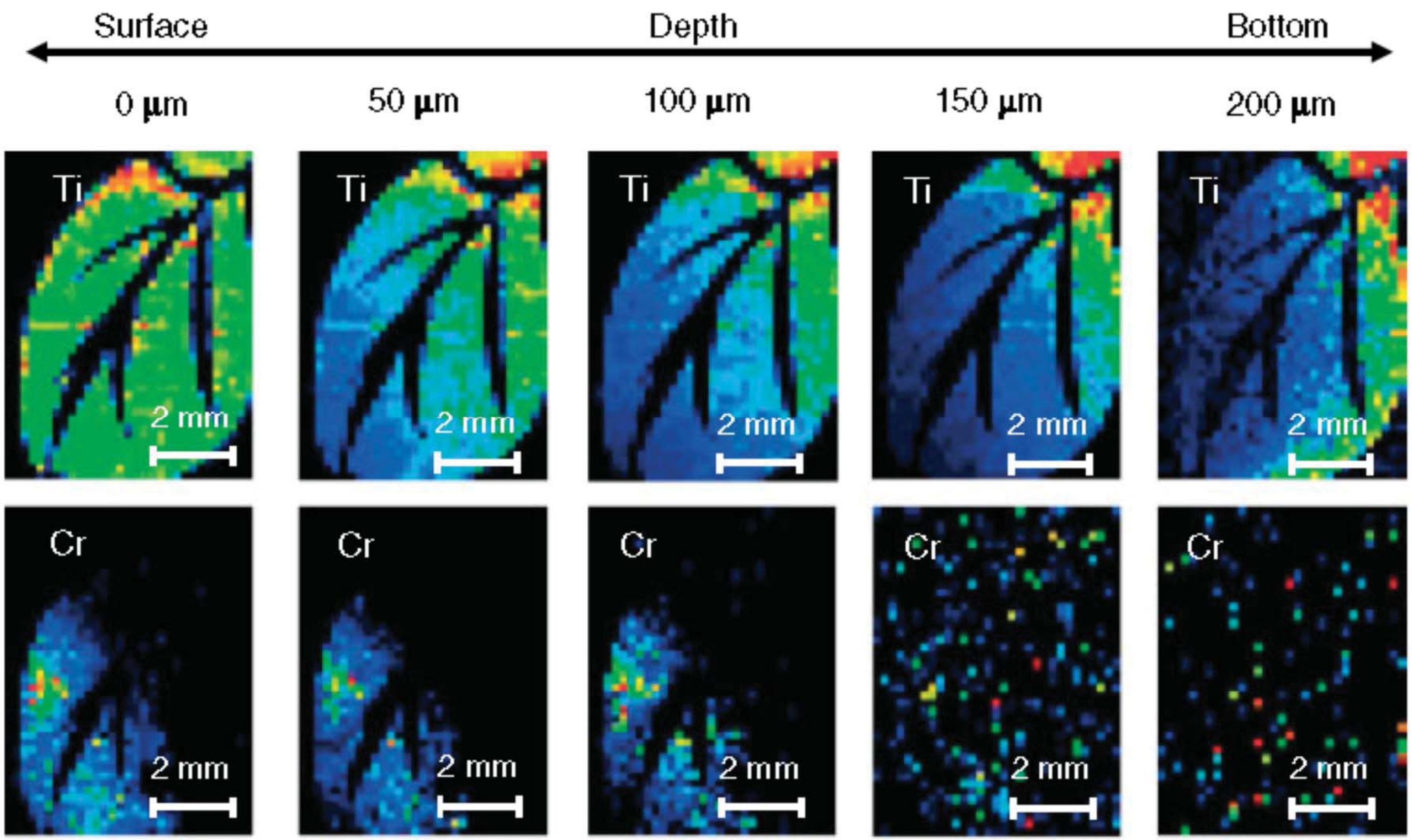

Nakano, Tsuji, XRS 2008, DOI 10.1002/xrs.1163

Elemental depth profiling of Japanese lacquerware 'Tamamushi-nuri'

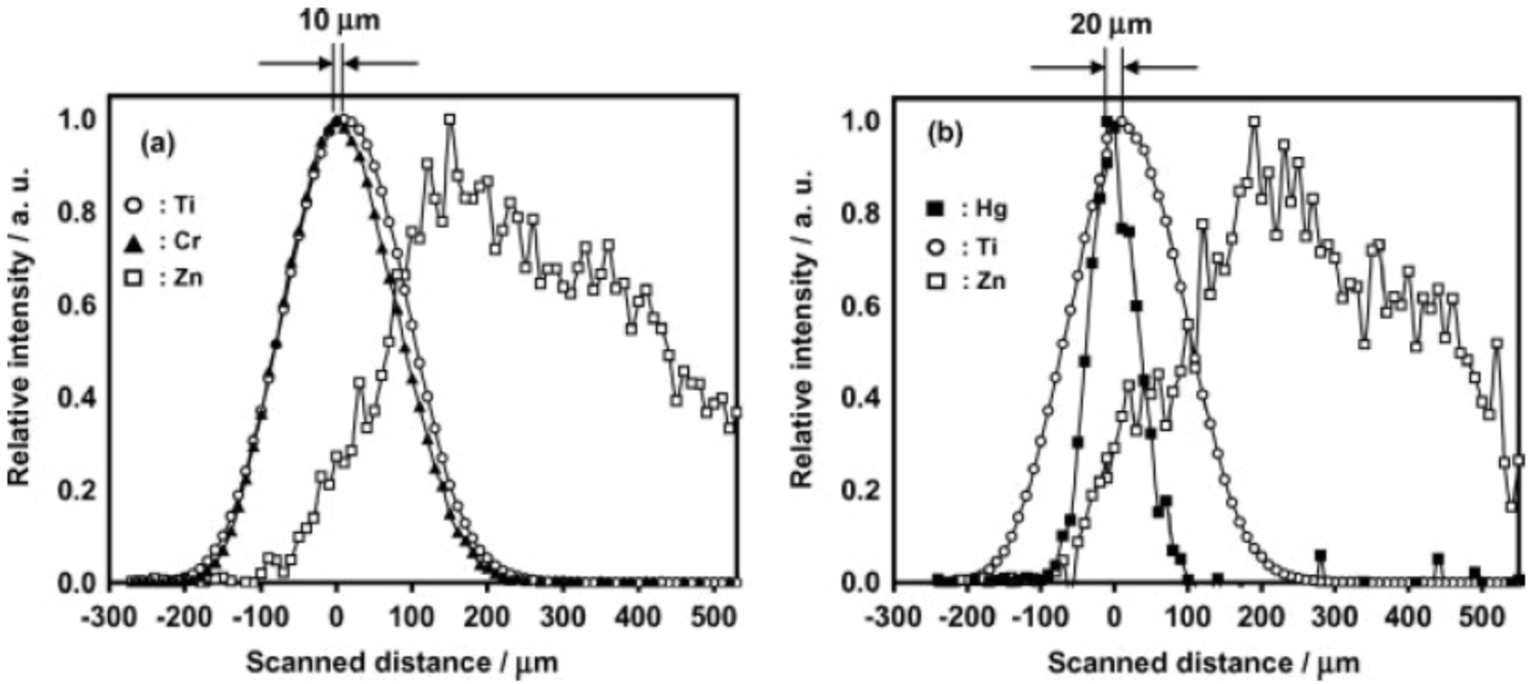

Nakano, Tsuji, XRS 2008, DOI 10.1002/xrs.1163

Portuguese polychrome glazed ceramics

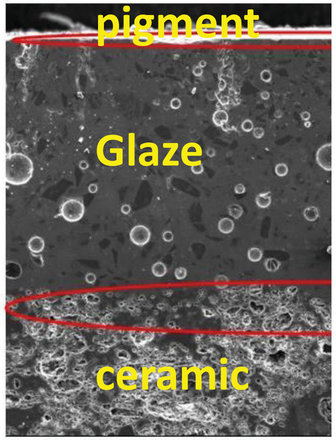

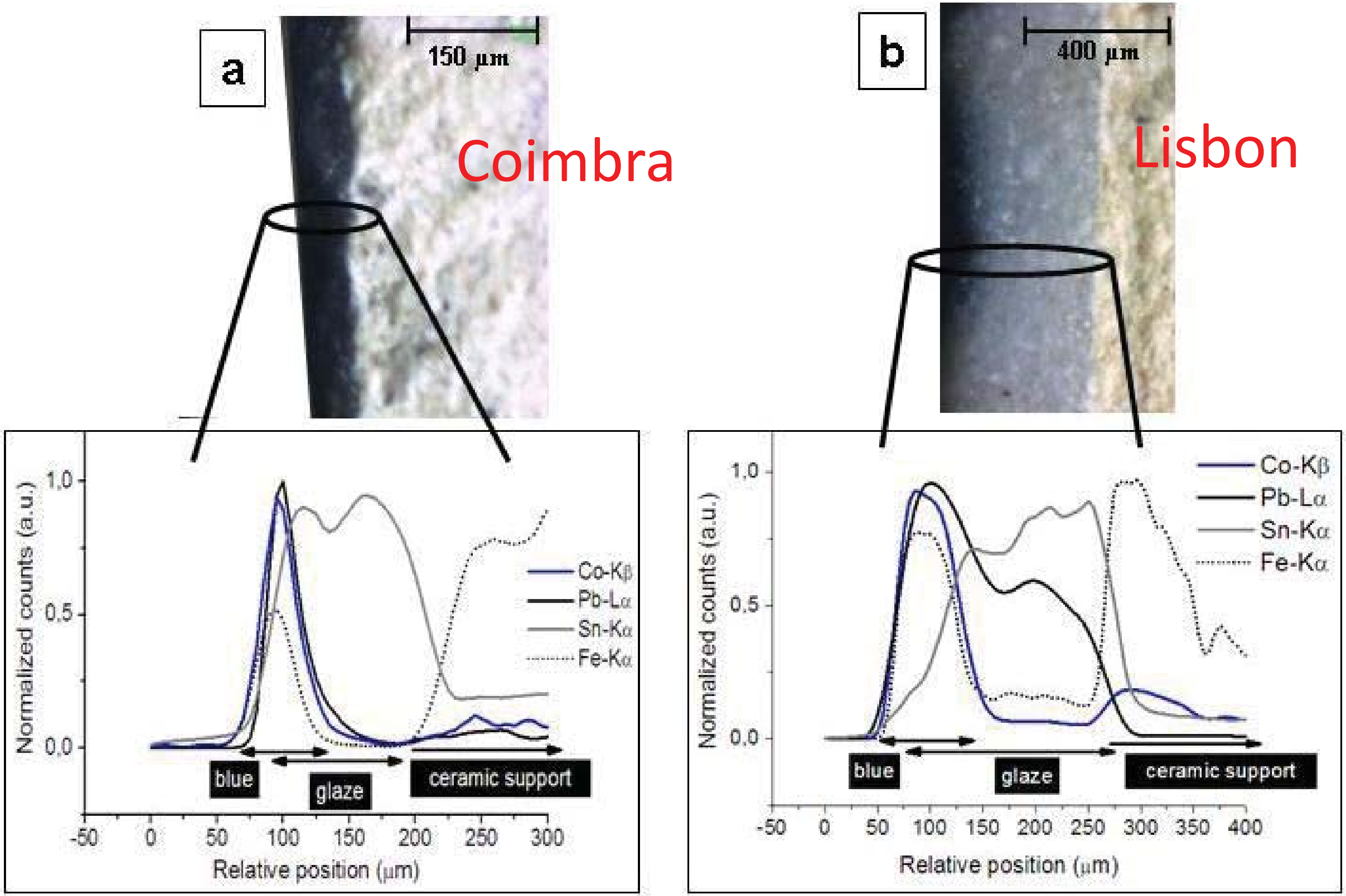

Guilherme et *al.*, **SAB 2011**

Combined 3D Micro-XRF/2D Micro XRF on the Dead Sea Scrolls

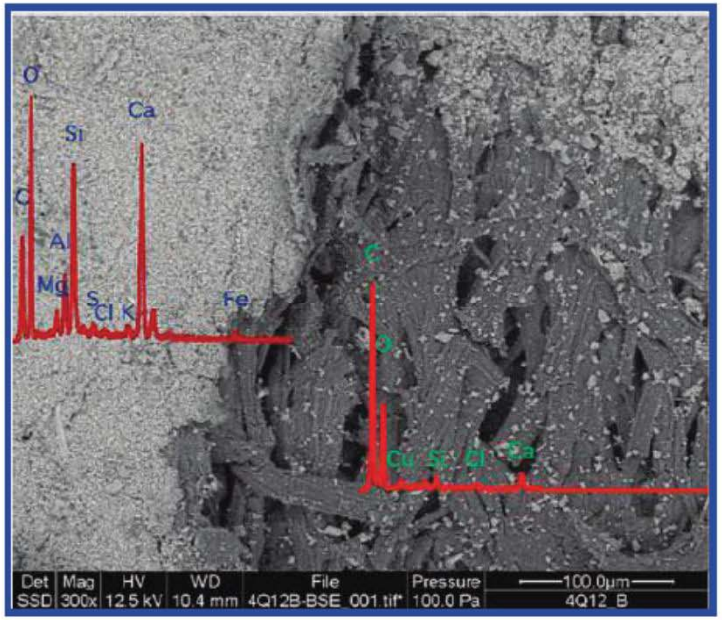

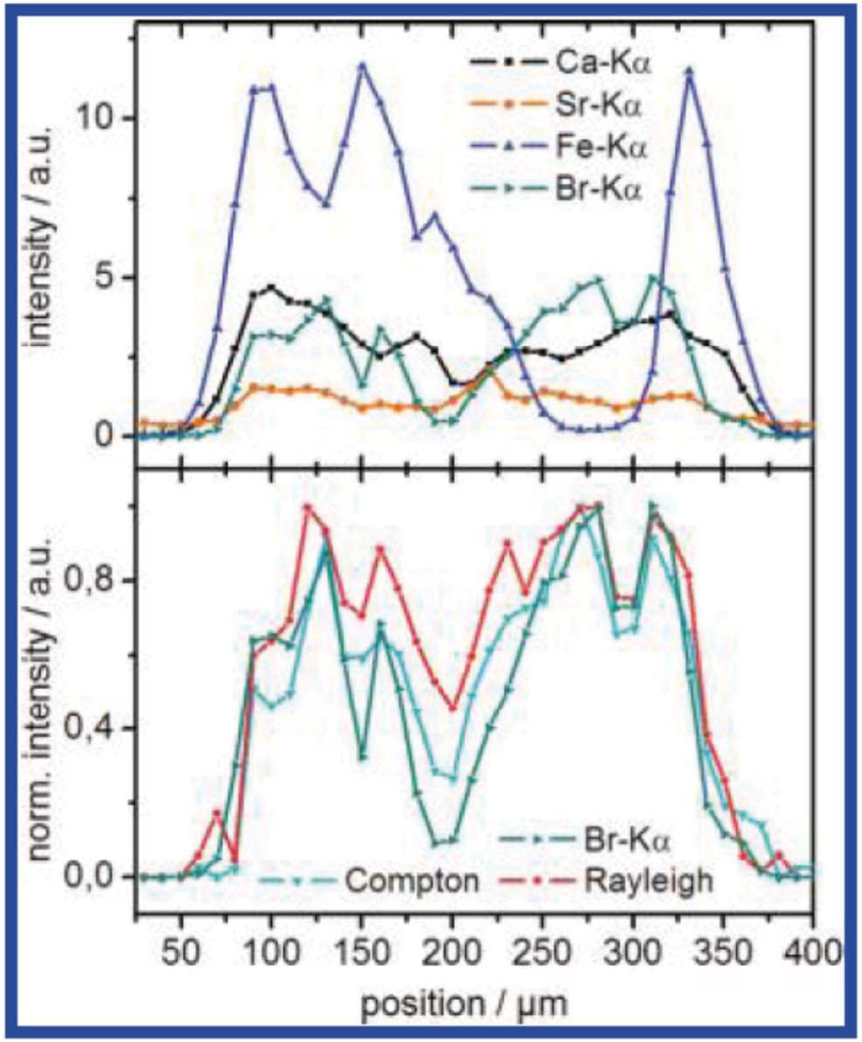

Mantouvalou et al Anal. Chem. 2011, 83, 6308–6315

Synopsis/Complementarily

Elements (Alumino-silicate matrix)	Techniques	Probing Depth	Concentration
Na - Cl	3D Micro -PIXE	<10-20 µm	Major
K-Zn	3D Micro -PIXE 3D Micro -XRF	<100 µm	Major/Minor Major/Minor
Ga – Ag, Au-U Ga - U	3D Micro –PIXE 3D Micro -XRF	<100 µm 100-300 µm	Major Major/Minor/Trace

Synopsis

➢The intensity profiles deduced from confocal depth scans incorporate composite analytical information such as the position and height of its centroid, the fwhm or actually the exact shape of the intensity distribution.

3D analysis may offer various analytical possibilities:

✓To resolve the features of a multilayered structure (elemental composition, thickness, layers)

✓To estimate concentration gradients

✓ Elemental composition of few tens um scale particles embedded mostly in a light matrix

Synopsis/Complementarily

Special features of 3D Micro-PIXE:

- ✓ One lens
- ✓ Easier alignment – Better overall set-up depth resolution
- ✓ The beam scanning mode provides fast and precise measurements
- ✓ The superior spatial resolution of the exciting beam offers element specific analysis of individual particles at the micrometer scale

Thank you for your attention!!

Acknowledgements

D. Wegrzynek, R. Padilla-Alvarez,
Ch. Apostolaki, Ch. Brecoulaki,
TUB group and B. Kanngiesser